Using a global magnetohydrodynamic model to study the start of the substorm recovery phase

N. L. Farr,[1] D. N. Baker,[1] and M. Wiltberger[2]

Received 14 June 2010; revised 14 September 2010; accepted 28 September 2010; published 16 December 2010.

[1] Magnetospheric substorms are a key manifestation of the transfer of energy from the solar wind to the Earth. Substorms consist of a loading of energy from the solar wind via magnetic reconnection and then a rapid release of that energy. One of the results of this energy release is the intense brightening of the aurora observed in the Earth's high-latitude regions. At some point, the dissipation of energy peaks and the system recovers. This paper focuses on addressing the question of what causes the transition to the recovery phase of the substorm typically defined by the retreat of the substorm magnetic reconnection site, or neutral line, in the magnetotail. One suggested hypothesis is that the expansion of the dipolarization of the magnetic field in the inner magnetosphere causes the neutral line to move tailward. We use the Lyon-Fedder-Mobarry magnetohydrodynamic code to model seven substorms to examine what causes the neutral line retreat in the simulation. We conclude that while the simulation reproduces the substorms with the loading and unloading of energy, the retreat of the neutral line is a directly driven process that is controlled by the solar wind.

Citation: Farr, N. L., D. N. Baker, and M. Wiltberger (2010), Using a global magnetohydrodynamic model to study the start of the substorm recovery phase, *J. Geophys. Res.*, *115*, A12237, doi:10.1029/2010JA015802.

1. Introduction

[2] Substorms are a collection of processes that transfer energy from the solar wind through the magnetosphere to the ionosphere. The explosive release of energy in the ionosphere results in the rapid brightening and then decay of the aurora. *Akasofu* [1964] was the first to identify and classify substorms from observations of these auroral brightenings. He identified two phases of substorms: the expansion phase, during which the aurora increases in size and brightness, and the recovery phase, when the aurora returns to its state during quiet times. Magnetospheric observations have been used by *McPherron et al.* [1973] to reveal that the "auroral substorm" was the ionospheric manifestation of the magnetospheric substorm and contains another phase, called the growth phase, which takes place prior to the expansion phase.

1.1. Growth Phase

[3] The growth phase is defined by the storage of energy from the solar wind in the magnetotail *Baker et al.* [1996]. When the IMF experiences a period of negative (southward) B_z, reconnection of the magnetic field occurs on the dayside of Earth. These reconnected field lines are then transported to the nightside due to the flow of the solar wind around the Earth's magnetosphere. The addition of this magnetic flux to the magnetotail results in a flared magnetotail with an increased amount of magnetic energy in the tail lobes. This increased energy density results in a greater pressure on the central plasma sheet, which causes it to thin. As it thins it still needs to maintain the current necessary to separate the north and south tail lobes and so the current density in the central current sheet increases. The magnetic field lines in the tail become much more stretched during this period. The increased amount of open magnetic flux also results in an increased size of the polar cap, which shows the area of the Earth's magnetic field that is connected to the IMF. The growth phase is 45–60 minutes in duration for a typical substorm.

1.2. Expansion Phase

[4] The expansion phase begins with an explosive release of the energy stored in the magnetotail during the growth phase. The exact cause of the onset is a matter of scientific debate with the two main theories being the Near-Earth Neutral Line (NENL) model [*Baker et al.*, 1996] and the Current Disruption (CD) model [*Lui*, 1996]. In the NENL model, substorm expansion phase onset occurs when the thinning of the plasma and current sheets in the magnetotail cause the current sheet to become thin enough that the oppositely directed magnetic field lines in the two hemispheres are close enough together for magnetic reconnection to occur resulting in the formation of the NENL. This reconnection X line brings magnetic flux in from the lobes and ejects plasma in the plasma sheet both earthward and tailward of the reconnection site. These flows in the plasma

[1]Laboratory for Atmospheric and Space Physics, University of Colorado at Boulder, Boulder, Colorado, USA.
[2]High Altitude Observatory, National Center for Atmospheric Research, Boulder, Colorado, USA.

0148-0227/10/2010JA015802

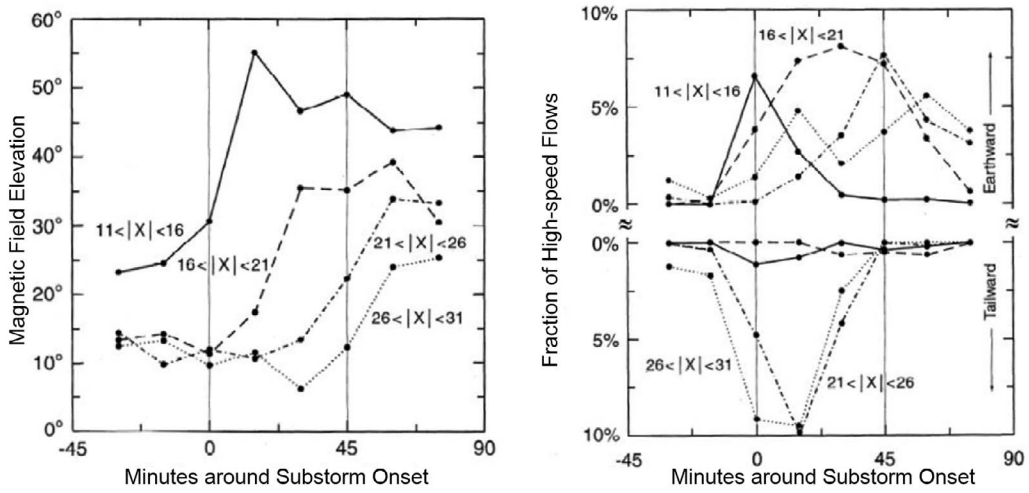

Figure 1. (left) The image shows the location of the dipolarization front in the magnetotail. (right) The image shows the percentage of high-speed flows observed in the tail, with the transition from earthward dominated to tailward dominated indicating the location of the neutral line. Adapted from *Baumjohann et al.* [1999].

sheet are high speed and the earthward flows quickly reach the inner edge of the cross-tail current sheet where they disrupt the current, creating the substorm current wedge (SCW). The current wedge then expands along the current sheet as well as tailward, diverting more of the cross-tail current into the ionosphere. This expansion of the SCW is also observed as a dipolarization of the magnetic field in this region. In the CD model, the thinned current sheet leads to a plasma instability at the earthward boundary of the plasma sheet which disrupts the crosstail current and sends a rarefaction wave tailward that initiates reconnection at the NENL.

[5] Tailward of the X line, a plasmoid forms at the location where the magnetic field lines are now forming a loop structure. Initially, the reconnection at the NENL begins on closed field lines and then proceeds to reconnect open field lines. Once this happens the plasmoid becomes surrounded by open field lines and begins to move tailward, leaving a thin plasma sheet between it and the X line. At some point, the X line starts retreating tailward marking the traditional transition from expansion to recovery phase. In the ionosphere the expansion phase is observed as a brightening of the aurora followed by an expansion of the auroral ring starting near midnight. Multiple brightenings can be observed during a single substorm.

1.3. Recovery Phase

[6] The substorm recovery phase is the period when the magnetotail and ionosphere transition from the expansion phase configuration back to quiet time conditions. It is the least studied aspect of substorms with most substorm research acknowledging it simply as a relaxation of the magnetotail back to normal conditions [*Opgenoorth et al.*, 1994].

[7] In the magnetotail the recovery phase is defined to begin when the X line begins its tailward retreat. In the ionosphere it is usually defined to begin with the start of the decay of the auroral electrojet or when the auroras reach their most poleward extent [*Pulkkinen et al.*, 1994]. The ionosphere definitions coincide fairly well, while usually preceding the X line retreat in tail [*Baker et al.*, 1994]. The time of peak power input into the ionosphere has been used to determine the start of the recovery phase [*Bryant*, 2008]. Key features of the substorm recovery phase are the rapid expansion of the plasma sheet and the presence of earthward flows in the midtail region. In the inner magnetosphere, the SCW decays and the field structure reverts to the quiet time configuration. Typically it begins about 45 minutes after substorm onset. In the inner magnetosphere, the SCW decays and the field structure reverts to the quiet time configuration. This reconfiguration can last for greater than 2 h.

[8] In the ionosphere, the recovery phase is signified by the decay of the substorm electrojet and the main auroral bulge. There is often an increase in activity in the morning sector and a second oval that appears poleward of the existing one. Sometimes recovery phase and expansion phase features can coexist for a substorm, suggesting that the recovery phase may begin locally and then become global [*Pulkkinen et al.*, 1991].

[9] One of the main questions regarding the substorm recovery phase is, what causes it to begin? Another related question is if a substorm is the magnetosphere's means of releasing the energy that is stored during the growth phase, then why does the recovery phase often begin while there is still free energy that has not been dissipated yet [*Baker et al.*, 1999]?

[10] One study that has sought to address the onset of recovery phase was *Baumjohann et al.* [1999] by performing a superposed epoch analysis of plasma sheet crossings by the Geotail spacecraft. They compared the flows observed with the magnetic field elevation angle, shown in Figure 1 and concluded that when a tailward-traveling dipolarization front reached the location of the X line,

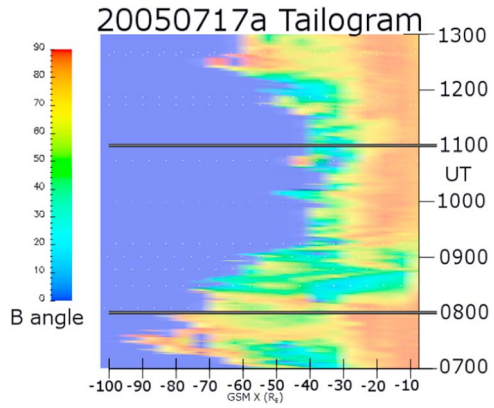

Figure 2. This is an example tailogram for the substorm 20050717a that displays the average magnetic dipolarization angle down the tail on the X axis and time along the Y axis. Dark blue represents locations that are tailward of the neutral at that time. The solid horizontal black lines indicate when the IMF turns southward and then northward. The color bar is showing the magnetic field angle with blue representing horizontal (and rare southward field) and red being a fully dipolar region.

it moves tailward to maintain the reconnection rate which occurs in a more stretched field region.

1.4. Overview

[11] Section 2 discusses the MHD model used in this paper as well as the unique analysis tool created to view the results. In section 3, the seven substorms used in this paper are presented along with comparisons between the simulation results and observations. A detailed walkthrough of the substorm cycle for one of the events is presented in detail. Section 4 presents analysis of several magnetospheric diagnostics to understand the substorm set. Section 5 presents the discussion and conclusions of this paper along with future work on this topic.

2. LFM

[12] This paper uses the Lyon-Fedder-Mobarry (LFM) MHD model to simulate several substorm events to determine what is the cause of the tailward retreat of the neutral line, indicating the start of the recovery phase. This section describes the MHD simulation used in this paper along with various tools used to draw information from its output.

2.1. LFM Model Description

[13] The LFM global MHD code has been in use for over 20 years simulating the Earth's magnetosphere and ionosphere system and its interaction with the solar wind [*Lyon et al.*, 2004; *Wiltberger et al.*, 2009]. The LFM model uses a modified spherical grid with a cylindrically shaped outer boundary. The inner boundary is at a distance of 2 R_E and maps along dipole field lines to an empirical ionospheric model. The outer boundary is at a distance of +30 R_E upstream and −300 R_E downtail with a radial distance of 100 R_E along the sides. The upstream and side boundaries use the solar wind input (provide by the ACE spacecraft for this study) as boundary conditions. The tail boundary condition is a simple outflow as the flow is supersonic at that distance.

[14] *Lopez et al.* [1998] used this simulation to study substorms and showed good agreement between the observations and the simulation for the onset, evolution, and second onset of the substorm sequence which occurred on 9 March 1995. *Wiltberger et al.* [2000] described the results from a substorm simulation for an event that occurred on 10 December 1996. They reported good agreement between geosynchronous magnetic field dipolarizations and the simulation results. Other global simulations of the magnetosphere including, *Raeder and McPherron* [1998], *Laitinen et al.* [2005], and *Toth et al.* [2005] have been used to simulate substorms.

2.2. Tools and Views of the Model Output

[15] In this section we discuss the different ways the model output is analyzed in this work. The basic tools used to represent simulation results are line plots and cutplane snapshots. Line plots show the temporal evolution of the system well, but are restricted to a single value for the system, while cutplane snapshots show a more global view but are restricted to single time.

[16] In global MHD simulations with no dipole tilt, the magnetosphere is mostly symmetrical in the z dimension and the current sheet is centered around the z = 0 plane, although tilting in the y direction can still occur [*Walker and Ogino*, 1996]. The version of the LFM used here including the dipole tilt, that is not always the case. The dipole tilt results in a current sheet with a hinge where the current sheet tilts from magnetic equator of Earth to being parallel to the Sun-Earth line. Another issue is variability in the solar wind direction which can cause the current sheet to tilt up or down in z as well. In addition magnetic structures traversing the tail cause the current sheet to distort away from a smooth plane on smaller scales as well. These factors all make using a single constant plane to monitor the current sheet in the tail inadequate at times. One solution that will be used in several images is a view of the current sheet surface which is formed by plotting the B_x = 0 surface in the magnetotail. This represents the center of the boundary between the north lobe and the south lobe.

[17] Another challenge with using the results from a fully three-dimensional magnetosphere simulation is to portray changes in the system over time in an efficient manner. Showing a series of cutplanes or other two-dimensional images at different times is an important way of understanding the evolution of the system. However, that approach becomes very bulky and awkward when looking at that system during multiple events; either the images are shrunk to fit on a single page, making it difficult to see some key features, or the series spans multiple pages, making it harder to observe the changes in the system. Line plots of single parameters are useful for making the information easy to see, but often it is important to see the spatial changes as well as the temporal ones. As a compromise in this conflict, one type of image that will be used in this paper is a "tailogram" shown in Figure 2. The x axis is distance tailward of Earth in R_E and the y axis is time in UT. The color bar is displaying the variable being mapped to this plot. For these tailograms, the current sheet surface, as described earlier, is used, except using only part of the surface with earthward

Table 1. Substorms Used in This Paper

ID	20050717b	20020811a	20050717a	20020811b	20050903a	20050903b	20051017
IMF B_z south (h)	1:30	1:47	3:05	4:27	5:39	7:19	7:28
Avg B_z (nt)	−3.9	−4.6	−7.3	−5.2	−3.2	−3.7	−2.9
Avg ρ (cm^{-3})	14.0	8.7	11.6	6.0	4.3	1.9	5.9
Avg V_x (km/s)	−441	−458	−475	−468	−648	−601	−376
Avg ϵ (10^{11} W)	4.5	4.1	6.6	4.3	6.1	4.9	1.4
Tot energy (10^{15} J)	2.5	2.7	7.3	6.9	11.2	12.8	3.9

flows, essentially the closed tail, and averaging it across they dimension in 5 R_E bins. In the example here, the mapped variable is the magnetic field angle, with red and orange being regions that are more dipolar and green and blue representing a more stretched magnetic field.

3. Events and Simulation Results

[18] This work studies four different intervals containing a total of seven substorms. Previous studies using MHD models to simulate substorm events have focused on reproducing a single event. This paper represents one of the largest substorm data sets simulated via MHD model. These events were chosen from Cluster observations of the plasma sheet in conjunction with AL observations of a substorm.

3.1. Solar Wind Driving Conditions

[19] The input for the simulations is the solar wind, as measured by the ACE spacecraft and propagated to Earth via ballistic propagation. B_z is the most significant solar wind parameter, as when it is negative, or southward, that reconnection takes place on the dayside of the magnetosphere. Then the reconnected magnetic flux is transported to the nightside of the Earth, which creates the conditions in the magnetosphere necessary to initiate a substorm. This section contains several plots of a variety of different variables for the seven substorms. They are displayed in the order of increasing duration of the southward B_z period that drove the substorm. Table 1 contains a list of the events with their start and end times and duration of southward B_z along with the average density, velocity, and B_z. Also displayed is the average value of the epsilon parameter,

$$\epsilon = \frac{|v|B^2}{\mu_0}\sin^4\left(\frac{\theta}{2}\right)\left(4\pi l_0^2\right) \quad (1)$$

where $\theta = \tan^{-1}(B_y/B_z)$ and $l_0 = 7 * R_E$, which is a proxy for the power transferred from the solar wind to the magnetosphere [*Koskinen and Tanskanen*, 2002], as well as the integral of epsilon parameter over the interval.

3.2. Substorm Walkthrough

[20] This section contains a detailed description of the evolution of substorm 20050717a as simulated by the LFM model. This substorm is representative of each of the substorms modeled in this paper. They all showed the same basic evolution: southward turning of the IMF, growth phase, expansion onset, period of tail reconnection activity, northward turning of the IMF, retreat of the neutral line, and recovery to quiet time conditions. At 0754 UT the IMF B_z component became negative and remained so until 1100 UT. During this time it had an average value of −7.3 nT.

[21] Figure 3 shows the IMF B_z component along with the virtual AL index. The vertical lines represent key times at which Figures 4–10 in the subsection will come from. Figures 4–10 contain four images to help show the substorm timeline. The upper left image is a noon-midnight cutplane, which displays the log of the density along with the last closed field (LCF) lines. In this image, the bow shock and magnetopause are visible as gradients in the density and the LCF lines show the size the closed field region as well as the amount of deviation away from a dipolar configuration. The most tailward point of the LCF lines is the X line where magnetic reconnection is taking place in the magnetotail. The upper right image is the same cutplane displaying the y component of the current density. In this image the bow shock and magnetopause currents are visible as blue arcs and the strength of the crosstail current is shown. The lower left image is the current sheet surface viewed from the north displaying the magnitude of the fluid velocity times the sign of V_x to indicate earthward versus tailward flow as well as the contour of $V_x = 0$. This most tailward part of the contour is the neutral line showing the transition from tailward flow to earthward flow. This is the same location as the X line from LCF image. The $B_z = 0$ contour could also be used in the magnetotail as it is usually colocated with the $V_x = 0$ contour. The velocity shows the strength of the flows in the magnetotail as well as their spatial distribution into flow channels. The lower right image is the same surface displaying the elevation angle of the magnetic field as well as

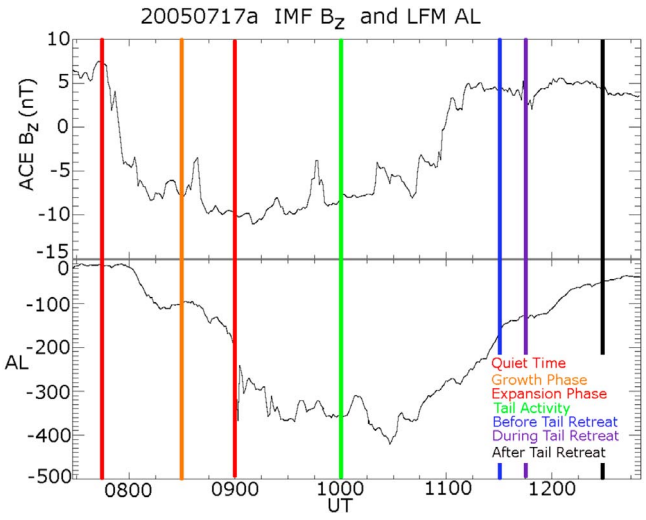

Figure 3. The IMF B_z and LFM AL index. The colored vertical lines indicate the times at which Figures 4–10 will show details of the substorm evolution.

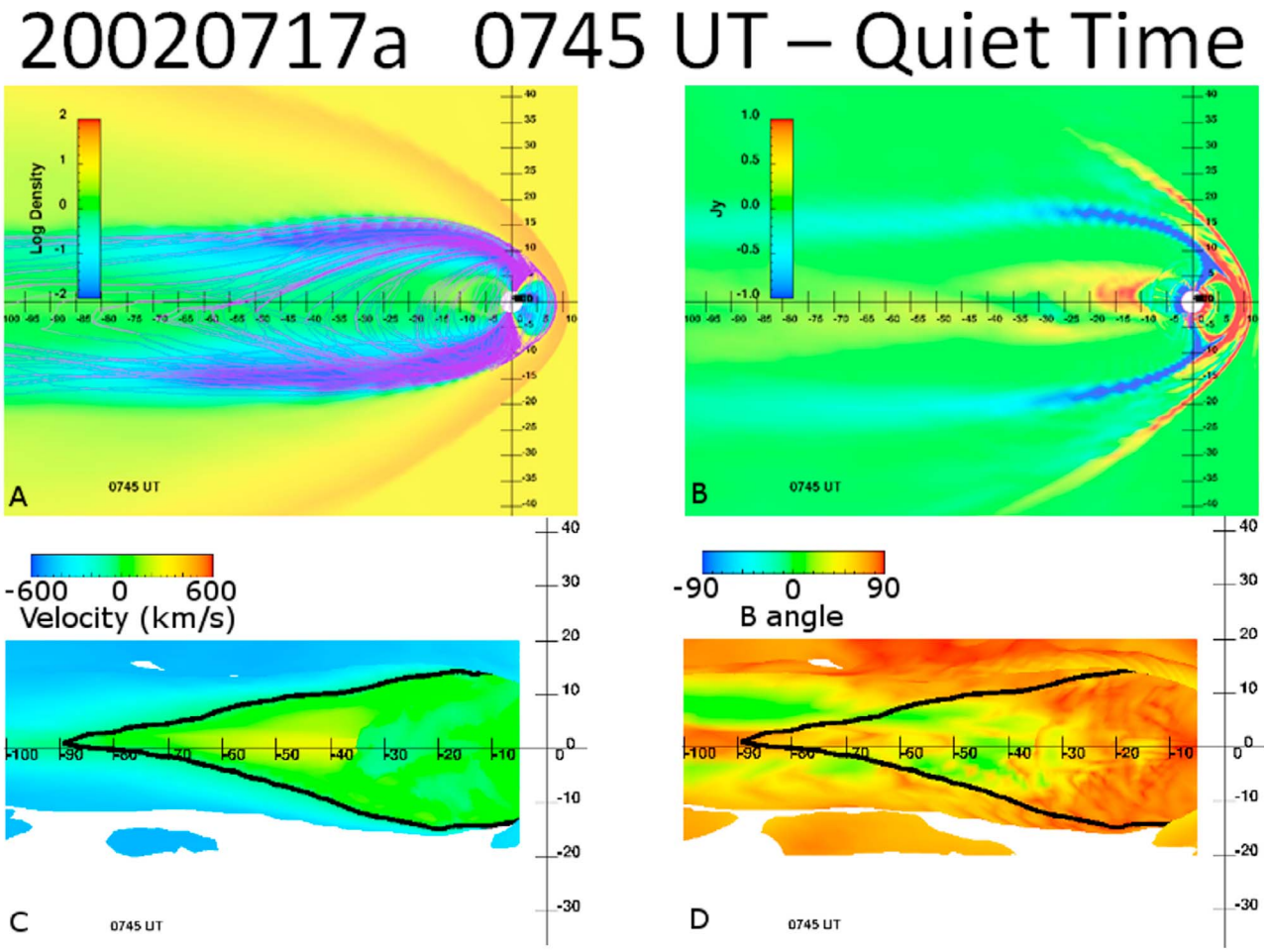

Figure 4. These four images show different views of the magnetotail before the substorm. See text for detailed description.

the V_x = 0 line. This image shows how the magnetotail magnetic field structure changes from dipolar to stretched and also relation between the location of the dipolar field and the neutral line.

[22] Figure 4 is from 0745 UT which is just prior to the IMF B_z turning southward. It shows the state of the magnetosphere at a nominal quiet time. Figure 4a shows that the volume of the closed field lines is large, with a radius of 15 R_E and extends far downtail. Figure 4b shows a weak cross-tail current that is only strong in the near tail region from −10 to −15 R_E. In Figure 4c there are no strong flows in the tail. The neutral line is at −90 R_E near midnight. In Figure 4d the magnetosphere is mostly dipolar out to −35 R_E and then more stretched further down the tail.

[23] Figure 5 is from 0830 UT during the growth phase. In Figure 5a the closed field region has shrunk considerably to a radius of 5 R_E and does not extend as far downtail as before. In Figure 5b there is a substantial enhancement in the crosstail current from the inner boundary out to past −40 R_E. In Figure 5c the neutral line has moved earthward to −65 R_E, but there are still no strong flows in the tail. In Figure 5d the stretching of the magnetic field is easily seen as there is essentially the entire tail has an magnetic field angle of <45°.

[24] Figure 6 is from 0900 UT shortly after expansion phase onset. In Figure 6a the closed field region has shrunk further and is composed of moderately dipole field lines earthward of −25 R_E and stretched lines tailward of that location. In Figure 6b the crosstail current is still quite strong, but it now exhibits structure earthward of −25 R_E. At that location there is a dropout in current strength in the y direction indicating a diversion or disruption of the current system. Figure 6c shows that the magnetotail is actually undergoing asymmetric behavior at this substorm onset. On the dawn side of the magnetosphere (y < 0), the neutral line is near −30 R_E with strong flows both earthward and tailward of the reconnection site. On the dusk side of the magnetotail, the neutral line is still located at −60 R_E, and there is now a region of strong earthward flow there as well. Following the flow channel earthward illustrates the diversion of these flows when they reach the near tail region. In Figure 6d there are now some areas of dipolarization at −20 to −25 R_E on dusk side and further earthward on the dawn side. Also on the dawn side at −60 R_E is another region of magnetic field reversal. This is the plasmoid flux rope that has been released and is moving tailward out of the system.

[25] Figure 7 is from 1000 UT, showing a representative time step during the period of southward B_z. In Figure 7a the

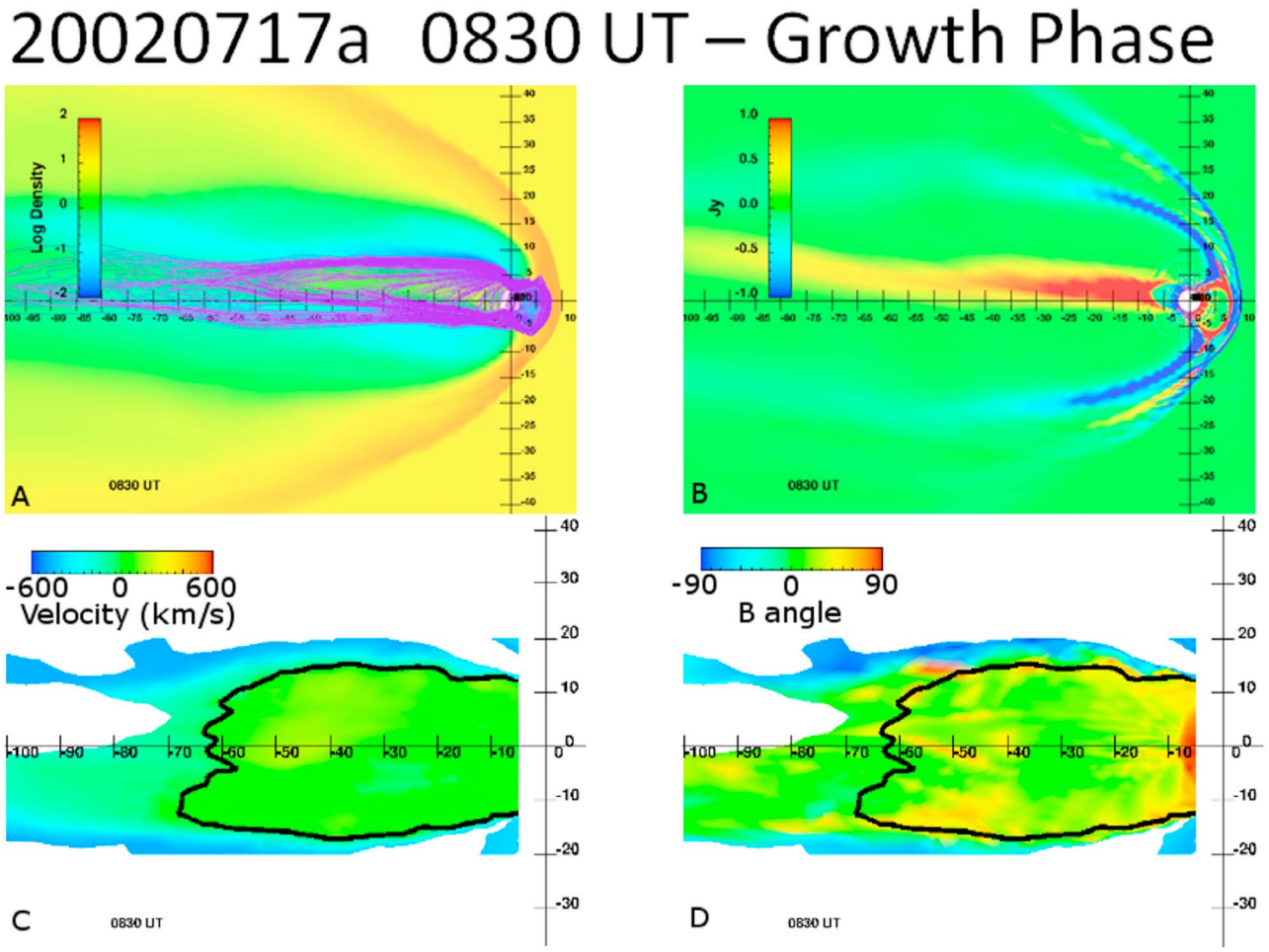

Figure 5. These four images show different views of the substorm during the growth phase. See text for detailed description.

closed magnetic field region remains small and dipolar. In Figure 7b the current maintains the structure with the diversion location at −20 R_E and substantial current in the near tail region. In Figure 7c the neutral line is now at −35 R_E and is mostly symmetric across the tail. The velocity shows moderate flows from that location that separate into three distinct flow channels at −20 R_E. In Figure 7d the magnetotail is very dipolar (angle > 60°) for the region earthward of −25 R_E and more stretched for last 10 R_E section of the tail.

[26] Figure 8 is from 1130 UT, which is after the IMF has turned northward, but before the retreat of the neutral line. In Figure 8a the closed field region has increased in the z dimension slightly, but is otherwise similar to before. In Figure 8b there is clear weakening of the crosstail current at all locations, although the structure is still visible and similar to the previous time. In Figure 8c the neutral line has not changed location, but the flows have weakened further leaving only two fainter flow channels. Figure 8d is similar to the previous one as the tail is dipolar earthward of −25 R_E and stretched tailward of that.

[27] Figure 9 is from 1145 UT. Figure 9a shows that LCF lines are now extending further tailward due to the X line retreat. Figure 9b shows that current continues to weaken, although it is still similar to before. In Figure 9c the neutral line has moved tailward to −50 R_E, which is a change of about 1 R_E per minute from the previous time. Also, the earthward flow is much weaker. Figure 9d shows the dipolar region of the magnetotail is still the same as before, but that newly closed portion of the tail is a stretched region.

[28] Figure 10 is from 1230 UT. Figure 10a shows that the closed field region has expanded back to roughly the size it was prior to the substorm. In Figure 10b the crosstail current is weak with just some activity in the near Earth region. Figure 10c shows the neutral line is at −75 R_E and no strong flows in the tail. Figure 10d shows the same dipolar near Earth region and more stretched tail.

3.3. Data Comparisons With LFM

[29] This section shows comparisons between the simulation and data. The comparisons with AL index are most useful for determining the overall timing of the substorm. The comparisons with the spacecraft are used for looking at the dipolarization of the inner magnetosphere.

3.3.1. AL Index Comparison

[30] Figures 11 and 12 show the comparisons between the AL index and a simulated one from the LFM simulation. Table 2 shows the correlation value and RMS error for each substorm. The four substorms from the events on 2002/08/11 and 2005/07/17 (Figure 11) are reproduced very well with

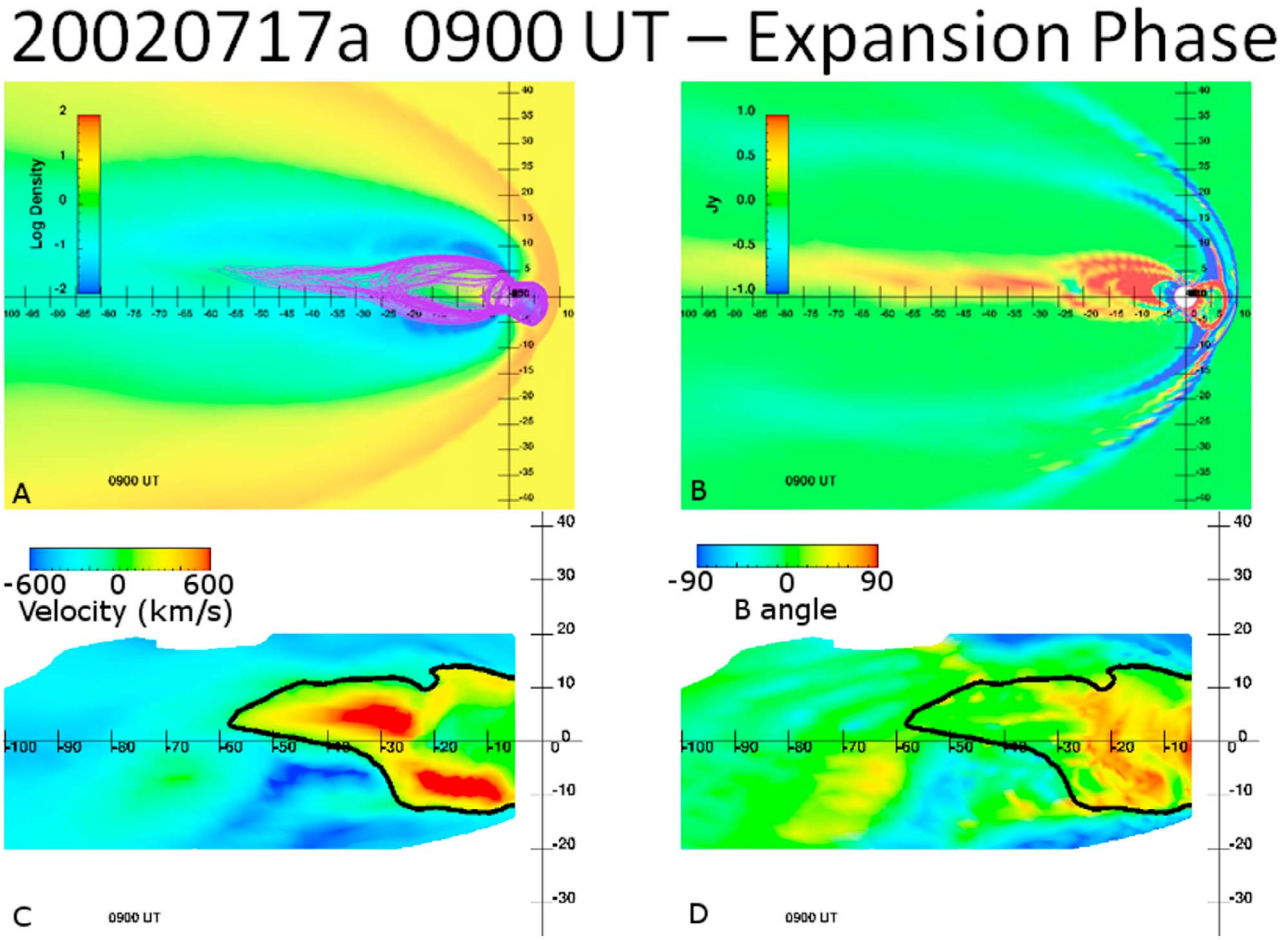

Figure 6. These four images show different views of the substorm during the expansion phase. See text for detailed description.

correlation coefficients of 0.76, 0.81, 0.94, and 0.78 and RMS errors of <150 *nT*, while the three substorms from 2005/09/03 and 2005/10/17 (Figure 12) are not reproduced as well with correlation coefficients of 0.65, 0.49, and 0.61 and RMS errors of >250 *nT*. The basic timing of the beginning and end of activity in the index is still reproduced. The simulated AL is systematically less than the actual data, especially during the peak of the activity. *Tanskanen et al.* [2001] found that 40% of the AL index during peak substorm activity was due to underground currents, which are not present in the simulation. The last column in Table 2 shows that for the first four substorms, the average simulated AL activity was within 40% of the real activity, so the missing underground currents could be an explanation for those events. For the last three substorms, the ratio of simulated activity to real activity is 30% and lower, so there must be an additional source for the lower levels of activity seen in the simulation.

3.3.2. Satellite Comparison

[31] Figures 13 and 14 show comparisons between satellite data and virtual satellites from the simulation. The plots are displaying the magnetic field elevation angle to show when the dipolarization is occurring.

[32] The satellite magnetic field angle for substorm 20050717a is shown in Figure 13. In Figure 13a, Cluster 1 saw dipolarization beginning at 0930 UT in the data and at 0900 UT in the simulation. For this event Cluster was very close to the dawn flank of the magnetosphere, and in the simulation the magnetopause was moving back and forth across the spacecraft resulting in the strong fluctuations in the magnetic field. In Figure 13b, GOES 12 saw dipolarization at 0910 UT in the data and at 0850 UT in the simulation. In Figure 13c, Polar saw dipolarization at 1015 UT in the data and at 1005 UT in the simulation.

[33] Figure 14 shows the satellite magnetic field angle for substorm 20020811b. In Figure 14a, Cluster 1 saw dipolarization beginning at 1500 UT in the data and at 1420 UT in the simulation. In Figure 14b, GOES 10 saw dipolarization at 1440 UT in the data and at 1410 UT in the simulation. In Figure 14c, Polar saw dipolarization at 1420 UT in the data and initially at 1400 UT in the simulation.

[34] Figure 15 shows the density and velocity at Cluster for substorm 20020811b. In Figure 15a, Cluster saw a peak in density followed by a sharp decrease at 1425 UT in the data and at 1355 in the simulation. In both data and simulation the peak density was 0.6 cc. In Figure 15b, Cluster saw a high-speed Earthward flow at 1447 UT in the data and 1426 in the simulation.

[35] Overall, the simulation did not reproduce the data from individual satellites as well as it reproduced the AL

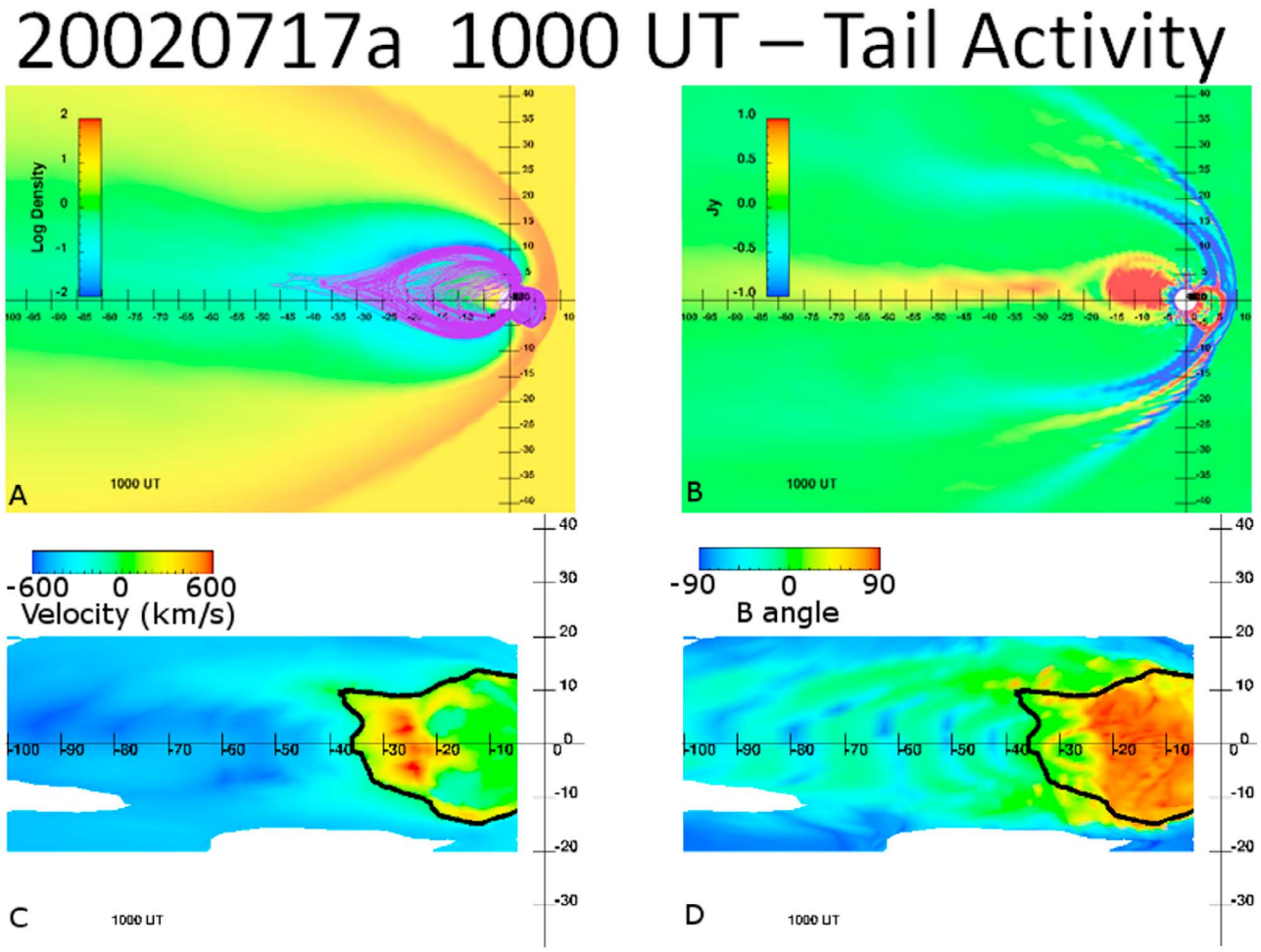

Figure 7. These four images show different views of the substorm during the period of tail activity. See text for detailed description.

index. The dipolarization signature was seen earlier in the simulation than in the data. This implies that either onset is occurring earlier in the simulation or the dipolarization of the inner magnetosphere spreads from the substorm current wedge spreads faster in the simulation, or both.

4. Analysis

[36] In the this section the tailogram view described in section 2.2 is presented for each substorm along with other magnetospheric diagnostics to understand the substorm cycle in the simulation.

4.1. Tailograms

[37] Figures 2 and 16 are the tailograms, as described in section 2.2, displaying the dipolarization of the tail averaged across the y dimension. In each event the tailograms show a fairly similar sequence. At the time of southward IMF, the neutral line is at the distant location of 60 R_E or more downtail. The magnetic field angle decreases throughout the tail, showing the stretching of the field lines that is occurring during the substorm growth phase. Approximately 45–60 minutes after the start of the growth phase, the neutral line makes a rapid jump earthward, representing the onset of the substorm expansion phase and release of the plasmoid. Throughout the remainder of the southward IMF, the neutral line remains in roughly the same location at about 30–35 R_E with some amount of fluctuation on the 5 R_E spatail scale used in these images. Then, about 30 minutes after the IMF turns northward, the neutral line begins to retreat back to the distant tail location.

[38] The tailogram for substorm 20050717a is shown in Figure 2. Shortly after the start of the southward IMF, the tail becomes stretched as indicated by the green and blue dominated tail. At about 0900 UT the tail becomes much shorter as the neutral line has moved earthward. Also the inner magnetosphere has become more dipolar again with most of the region earthward of −30 R_E having an magnetic field angle > 75° as shown by the orange and red area. The tail then remains in a similar state until about 1130 UT when the neutral line begins to move tailward, increasing the size of the closed magnetotail. At the beginning of this tailward retreat, the newly closed tail region is still stretched in comparison to the inner magnetosphere. At about 1220 UT this changes with full closed tail region becoming dipolar.

[39] Figure 16 shows the tailograms for the other six substorms. In Figure 16a the tailogram for substorm 20020811a is displayed. From the time of the initial southward

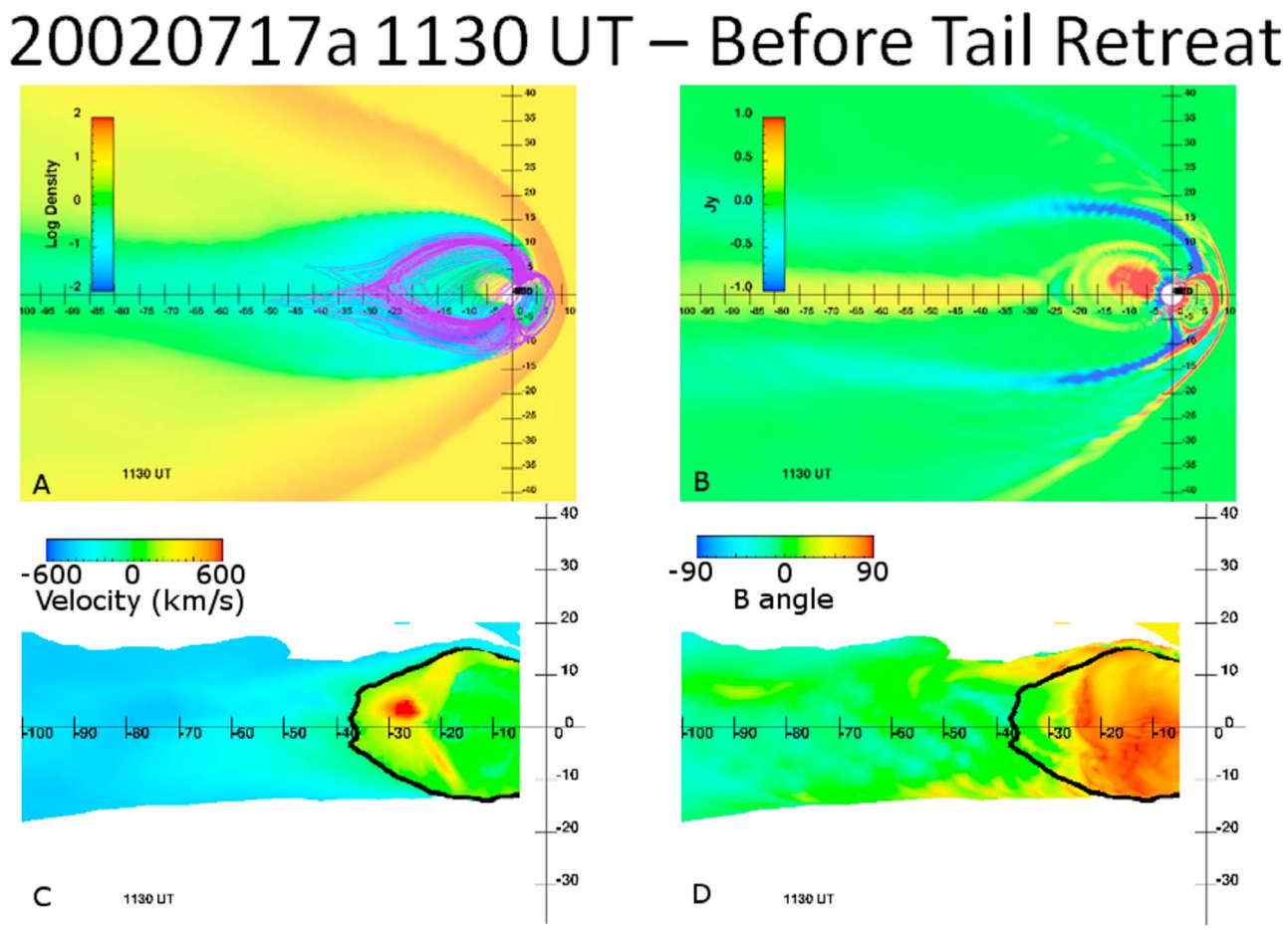

Figure 8. These four images show different views of the substorm prior to the tail retreat. See text for detailed description.

IMF, the tail becomes more stretched until 1050 UT when the neutral line begins moving earthward. At this time the inner magnetosphere becomes dipolar out to −30 R_E. At 1230 UT the neutral line begins moving tailward again, remaining stretched tailward of −30 R_E until it reaches the location of −70 R_E, and the whole closedtail becomes more dipolar at 1250 UT.

[40] Figure 16b shows the tailogram for substorm 20020811b. At 1330 UT the tail becomes stretched and at 1400 the neutral line moves earthward to −35 R_E with the inner magnetosphere dipolar earthward of −30 R_E. This state persists with fluctuations in the location of the neutral line until 1800 UT at which point the neutral line retreats tailward to −80 R_E.

[41] In Figure 16c the tailogram for substorm 20050903a is shown. At 0000 UT the neutral line moves earthward. This substorm does not show substantial stretching of the magnetic field in the inner magnetosphere prior to substorm onset. During this substorm there is more motion of the neutral line than the other substorms prior to 0530 UT when it retreats to −100 R_E.

[42] Figure 16d shows the tailogram for substorm 20050717b. At 1400 UT the neutral line begins moving earthward to −35 R_E and stays there until 1520 UT when it begins to move tailward. The initial part of the tailward retreat is not accompanied by a dipolarization of the tail, but after the neutral line reaches a distance of −60 R_E the entire closed tail becomes dipolar.

[43] The tailogram for substorm 20050903b is displayed in Figure 16e. After the southward IMF, the inner tail becomes slightly more stretched into −15 R_E. At 0730 UT neutral line undergoes an extreme jump in location, moving from >100 R_E to −30 R_E. The inner magnetosphere earthward of −35 R_E becomes dipolar again. Like the previous substorm the neutral line has a lot of variation throughout the period of southward IMF. At 1430 UT, the neutral line begins moving tailward while the newly closed tail remains stretched until 1600 UT at which point the entire closed tail dipolarizes.

[44] Figure 16f shows the tailogram for substorm 20051017. After the southward turning of the IMF, the tail stretches with the neutral line remaining at −60 R_E. At 1100 UT the neutral line begins moving earthward with the inner magnetosphere becoming dipolar again. The neutral line remains at −30 to 40 R_E until 1900 UT when it moves tailward again.

4.2. Magnetospheric Diagnostics

[45] Figure 17 shows the polar cap area for each substorm in this paper. The vertical blue lines show the start and stop times for the intervals of southward IMF for each substorm. The vertical red line shows the time when the initial

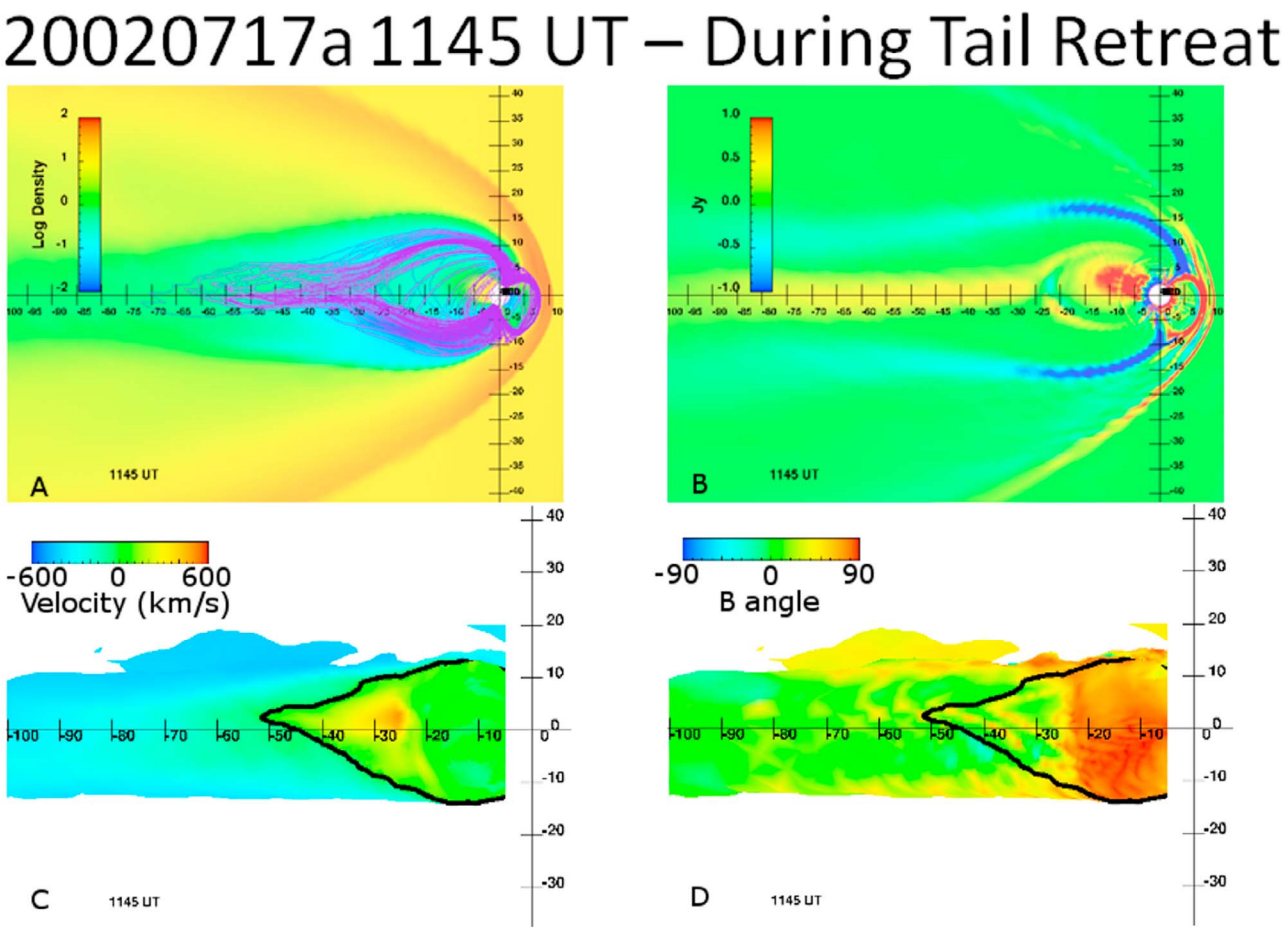

Figure 9. These four images show different views of the substorm during the tail retreat. See text for detailed description.

expansion of the polar cap ended. This is one sign of the end of the growth phase and the transition to the expansion phase as it indicates that reconnection in the magnetotail is now removing more magnetic flux from the open polar cap than reconnection on the dayside is adding open magnetic flux. For five of the substorms (Figures 17a–17d and Figure 17f), the initial growth of the size of the polar cap is marked by a peak, followed by a decline. For the other two substorms (Figures 17e and 17g) the size of the polar cap levels off and then increases further at a later time. Periods of relatively stable values for the polar cap indicate that the rate of reconnection in the tail is balanced with the reconnection on the dayside. The average duration of the growth phase as delineated by the initial expansion of the polar cap is 61 ± 11 minutes. The average value for the size of the polar cap at the end of the growth period is 0.26 ± 0.04 R_E^2. This is in agreement with observations of the polar cap area by *Brittnacher et al.* [1999] which measured the maximum polar cap area for three substorms to be 0.20, 0.25 and 0.29 R_E^2.

[46] The substorms in Figures 17a and 17b are easily grouped together, in that they both show fairly symmetric peaks with the rate of decline being similar to the earlier rate of increase. Conversely the other substorms (Figures 17c–17g) show a slower decline, especially prior to the northward turning of the IMF after which the second group of substorms shows a steeper decline in area when compared to the period prior to the northward turning. Another feature to note is that the substorms on Figures 17e and 17f both show a smaller, but noticeable, increase midway through the substorm. This is probably related to the very brief periods during those events when the IMF turns northward for short intervals. These northward turnings do not lead to a recovery of the system, but could be inducing a secondary substorm onset in the midst of the larger substorm.

[47] Figure 18 shows the size of the plasma sheet in the z dimension at −20 R_E for each substorm. The vertical blue lines show the beginning and end of each period of southward IMF. The vertical red line indicates the time of the minimum thickness. For the purpose of this calculation the plasma sheet is defined as the region of the magnetotail that is on closed field lines and has a plasma beta greater than one. Each substorm here shows a thinning during substorm growth phase. The average duration of thinning after the start of southward IMF is 48 ± 10 minutes. The average thinning experienced was from 15 ± 4 R_E to 4 ± 2 R_E. This is not as thin as observations of the plasma sheet which find that it can reach a size of <1 R_E [*Petrukovich et al.*, 2007]. The grid resolution in the tail could be having an effect of this difference. The plasma sheet then stayed at roughly that thickness for the remainder of southward IMF before thickening again after the IMF turned northward.

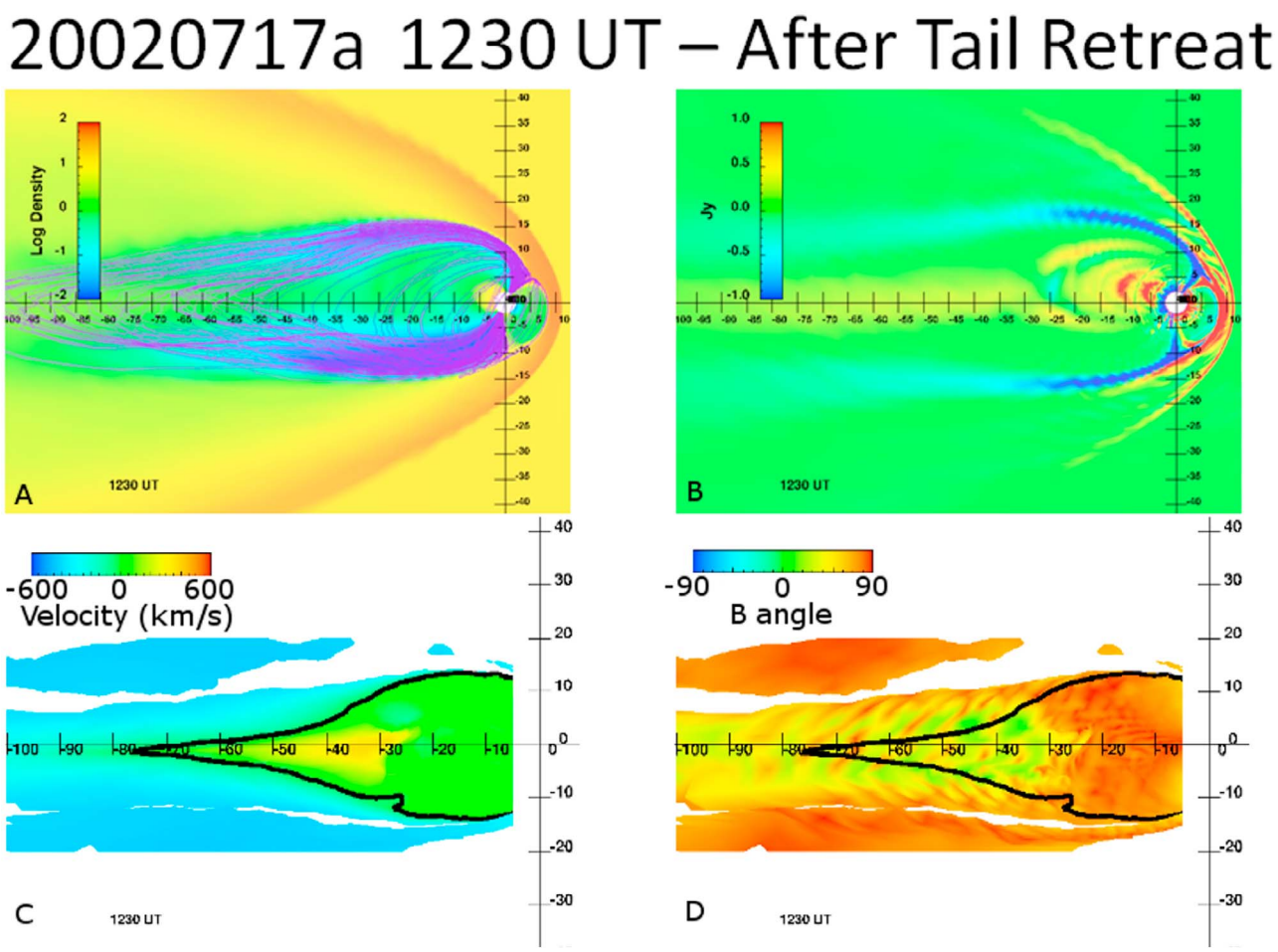

Figure 10. These four images show different views of the substorm after the tail retreat. See text for detailed description.

[48] The location of the neutral line for each substorm is shown in Figure 19. The neutral line for this plot is defined to be the location of earthward flow that is furthest from Earth in the current sheet. Two times are highlighted on the plots: a vertical red line indicating the time of the earthward jump of the neutral line that occurs at substorm expansion onset and an orange line indicating the start of the neutral line retreat, indicating the beginning of the recovery phase in the magnetotail. This usage of the neutral line is somewhat complicated during the release of the plasmoid as the Earthward jump in location is only seen when the entire plasmoid begins moving tailward and not at the time of the initial near-Earth reconnection which begins the process of plasmoid creation. As this is a single value for the tail, the asymmetry shown during the substorm walkthrough in section 3.2 is obscured as well. Therefore, a time at the beginning the strongest earthward motion is chosen to be the onset of the NENL. The identification of the time of tailward retreat is more simple as it is the point at which a tailward motion begins that does not make a relatively quick return to the near-Earth location. The substorms in Figures 19d–19g all show fluctuation in the of the neutral line during the substorm, but the values return to the near-Earth location. The average time from start of southward IMF to the earthward jump of the neutral line is 54 ± 14 minutes. The retreat for the neutral line takes place after the northward turning of the IMF in every substorm, and the average length of time from the northward turning to the retreat of the neutral line is 20 ± 8 minutes.

5. Discussion

[49] This paper has used the LFM MHD simulation to show that the substorm recovery phase is a process that is directly driven by the solar wind. When the southward IMF that drives the substorm cycle is turned off, the substorm begins the recovery back to the quiet time conditions. This is in contrast to growth phase and expansion onset which are shown to be a process of energy loading and unloading that is determined by the internal configuration of the magnetosphere.

5.1. Comparison of the Simulation Results With Data

[50] When using a model to simulate real events it is important to validate the simulation results against data for the events to have a level of confidence in the ability of the model to simulate the real system. This paper uses the AL auroral index as the primary means of comparing the simulation with the data. The reasons for using the AL index are that it is a traditional means of identifying the occurrence of

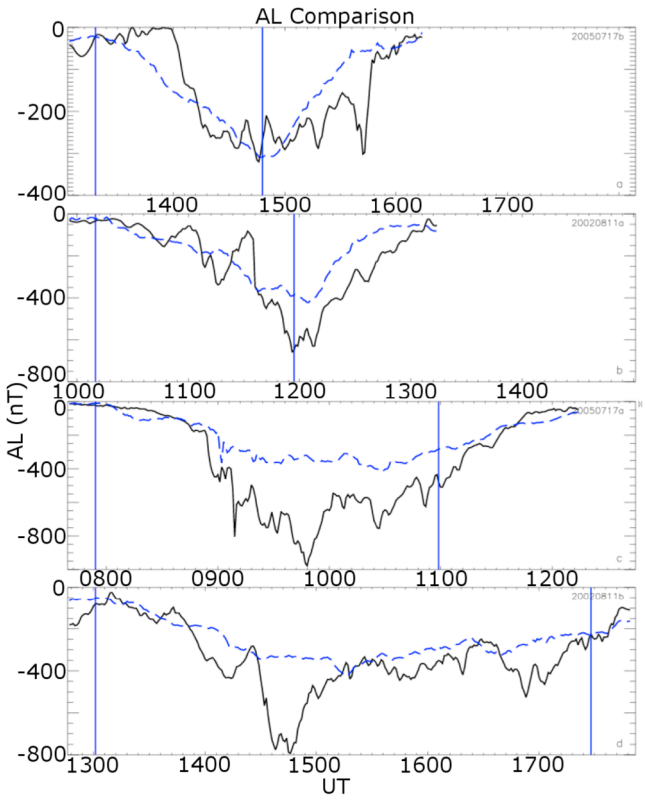

Figure 11. Shown are the AL comparisons for substorms 20050717b, 20020811a, 20050717a, and 20020811b. The AL index from the Kyoto World Data Center is shown as the black solid line and a simulated index calculated from the LFM simulation is shown as the blue dashed line. The two vertical lines represent the start and end times for the period of southward B_z for the substorm.

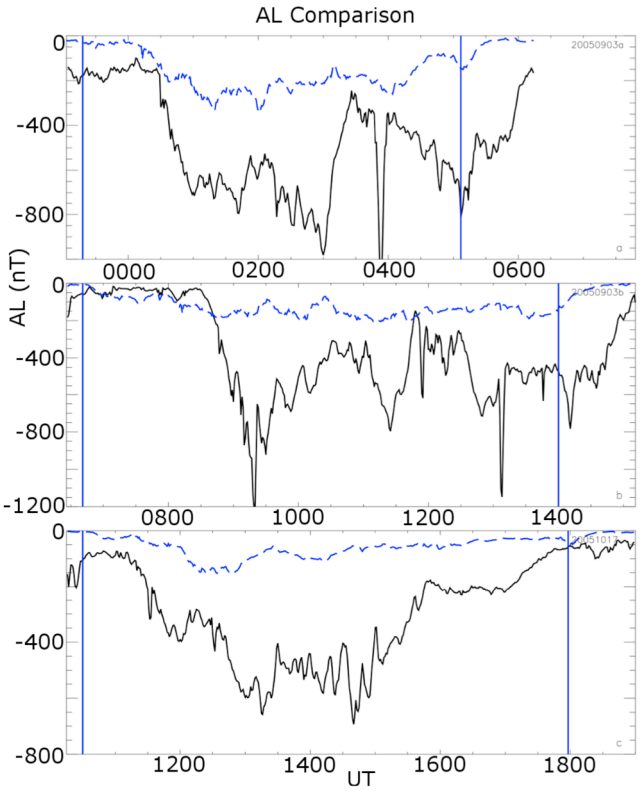

Figure 12. Shown are the AL comparisons for substorms 20050903a, 20050903b, and 20051017 in the same format as Figure 11.

substorms as defined by their change to the auroral current structure and that it is a global value that is less affected by localized variation when compared to other measurements like data from an individual spacecraft. As described in section 1, the SCW diverts a portion of the inner part of the cross-tail current into the ionosphere. These enhanced ionosphere currents create significant deviations in the magnetic field at Earth that are observed by the ground magnetometers which are used to generate the AL index.

[51] In section 3.3, Figures 11 and 12 show the comparison of the data from ground magnetometers with the virtual version computed from the LFM simulation. The AL comparisons show that the global nature of the substorm activity is reproduced fairly well by the simulation, with some substorms reproduced better than others. The simulations of substorms 20050717b, 20020811a, 20050717a, and 20020811b (Group A) all reproduce the AL index with correlation values of 0.76, 0.81, 0.94, and 0.77, respectively. They also each reproduce more than 60% of the amount of activity measured by the index. In contrast, substorms 20050903a, 20050903b, and 20051017 (Group B) do not reproduce the AL index as well. The timing of the substorms, as represented by the correlation values of 0.65, 0.49, and 0.61, show that timing of the substorms is adequate, but not as good as Group A. The performance aspect that is the worst for these events is that the average activity during the substorms in the simulated AL index is only 30% or less of the average activity level of the data AL index. This means that the ionosphere currents being generated by the simulation for these events is considerably weaker than the real currents.

[52] Looking at the solar wind driving conditions to explain the difference in performance between the two groups, only the B_z yields a strong correlation to the ratio of simulated activity to data, with a value of −0.63. However, the primary variable used for the driving of the magnetosphere by the solar wind is the epsilon parameter, which is an estimate of the incident power from the solar wind into the magnetosphere and the correlation between epsilon and the activity ratio is only 0.25. This makes sense in that substorms 20050903a and 20050903b are the second and third strongest driven substorms in this data set and

Table 2. Correlation Between the Real AL Index and the Simulated One

ID	Correlation	RMS Error	Ratio of Simulation Avg to Data Avg
20050717b	0.76	53.1	0.93
20020811a	0.81	99.5	0.76
20050717a	0.94	143.7	0.61
20020811b	0.78	91.0	0.75
20050903a	0.65	333.2	0.30
20050903b	0.49	271.7	0.29
20051017	0.61	266.5	0.15

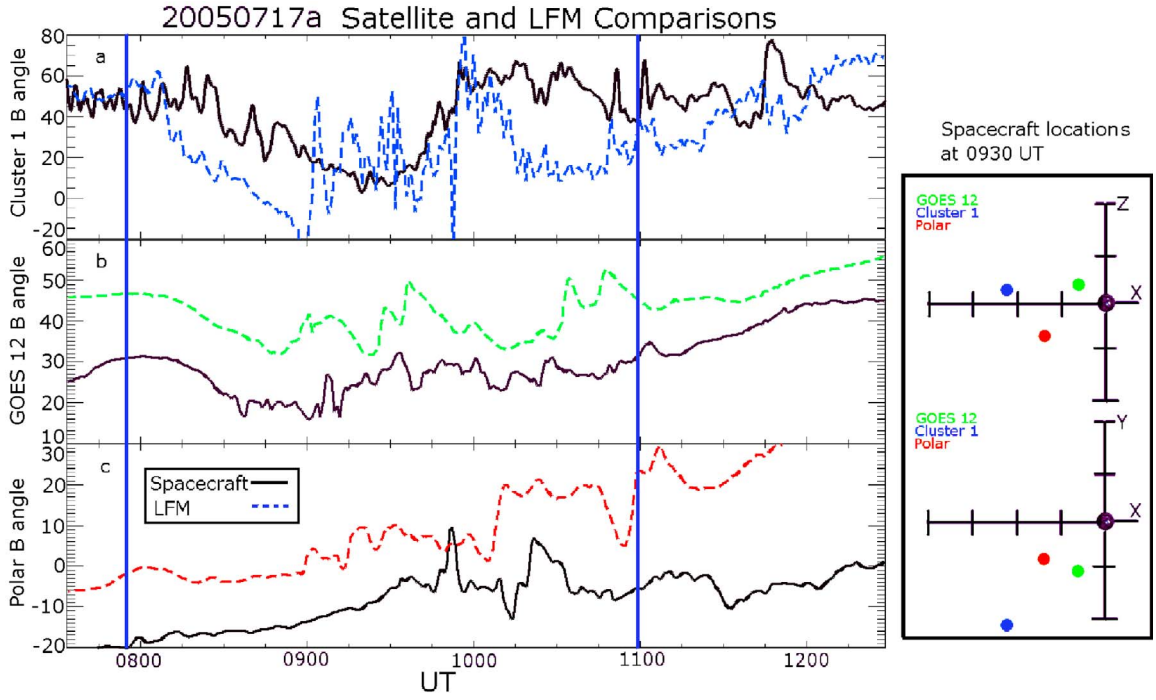

Figure 13. This plot is for substorm 20050717a: (a) Cluster 1, (b) GOES 12, and (c) Polar. All plots are showing the magnetic field angle with the data shown in solid black lines and the simulation results are shown in dashed colored lines. The vertical blue lines are the beginning and end times of the southward IMF.

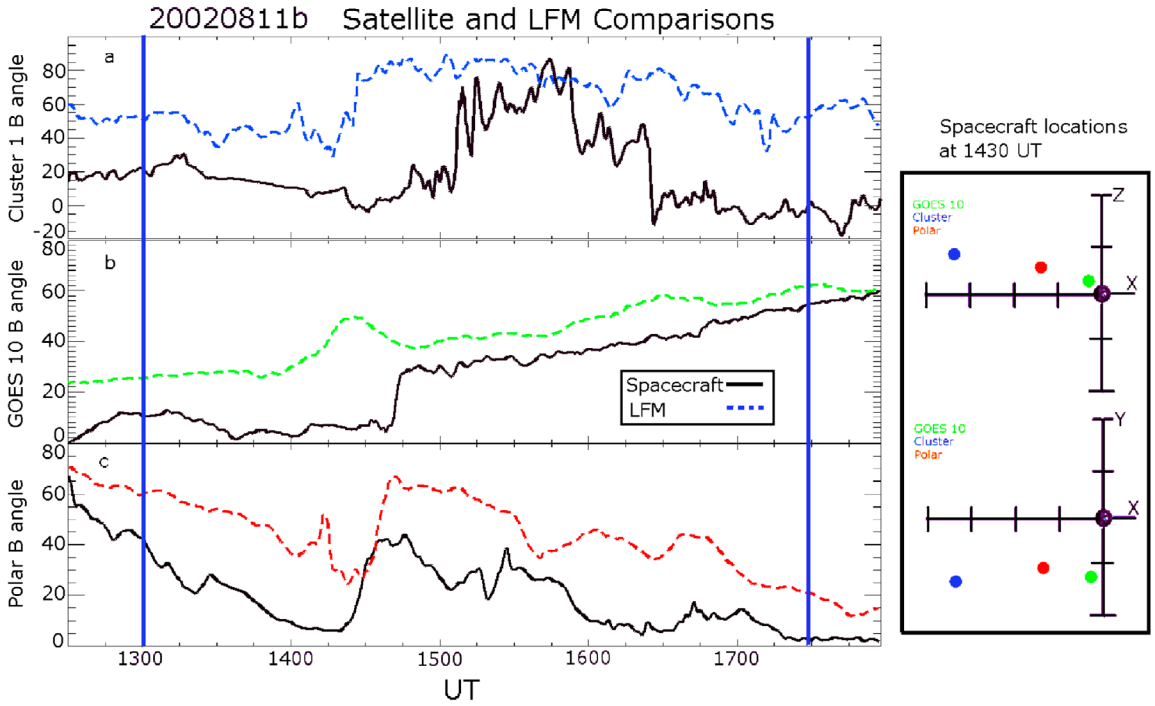

Figure 14. This plot is for substorm 20020811b in the same format as Figure 13.

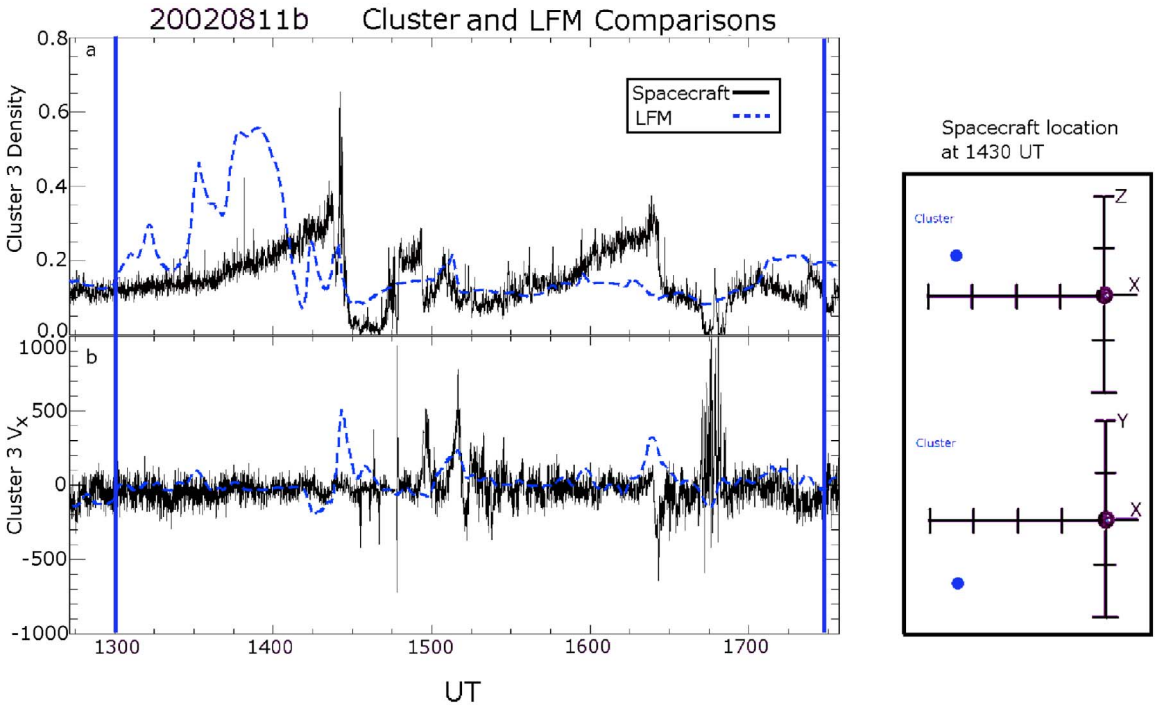

Figure 15. This plot is for substorm 20020811b: (a) Cluster 3 ion density and (b) Cluster 3 ion velocity. The data are shown in solid black lines, and the simulation results are shown in dashed blue lines. The vertical blue lines are the beginning and end times of the southward IMF.

20051017 is the weakest. Another cause to consider is that the substorms in Group B are the three with the longest periods of southward IMF in the paper. This cause is ruled out by the fact that poor performance of the simulation for these events is present in the early part of the simulation run, which has no information about how long the event will last. Had the IMF turned northward at a much earlier time, they still would have been poor performers. Finally, the substorms in Group A are from just 2 days while the substorms in Group B from a separate set of 2 days, which suggests the possibility that there is something about the events themselves leading to the differences in performance.

[53] Two possible reasons for these could be the following: the time of year of the events, or the accuracy of the solar wind propagation from the ACE spacecraft at L1 to Earth. For the former explanation, it is noticed that Group A takes place on days (17 July and 11 August) nearer the solstice while the events comprising Group B take place on days (3 September and 17 October) that are closer to the equinox. If there is something in the simulation that treats the relative differences between these times different than they are in reality, then it could shed light on the different performances observed here. In regards to the propagation of the solar wind data from the L1 point to Earth, comparisons between the propagated data and data measured just upstream of Earth have shown that the propagated solar wind is a good measure of the actual solar wind parameters that impact Earth's magnetosphere [*Weimer et al.*, 2003]. But with the small sample size here, it is possible that, for the events comprising Group B, the propagated solar wind is not as accurate of a proxy.

[54] The comparisons of the simulation results for the virtual satellites with the data is not as good as it is with the AL index. There are two main sources of error in these types of comparisons. The first is that the spacecraft are generating point measurements and given the size and variability seen in the earthward flowing flow channels, it is not likely that the simulation would reproduce these small-scale structures in exactly the same place and times for them to be seen by virtual spacecraft. The other consideration is a systematic one, where the location of the NENL in the simulation (−30 to −40 R_E) is not as close to Earth as is typically seen in the data (−20 to −30 R_E). Also, the current strength in the inner magnetosphere is not as strong in the simulation as it is in the data. These weaker current strengths mean that the magnetic field in the inner magnetosphere is more dipolar than it is in reality.

[55] Since the key criteria for the onset of reconnection at the NENL is the very thin current sheet with oppositely directed magnetic field lines, this lower level of stretching and weaker currents in the inner magnetosphere mean that the location for the NENL will be further downtail where the currents and stretching are sufficiently strong enough for it to occur. These issues could lead to the SCW being further out from Earth when it is formed, which would lead to the initial dipolarization of the inner magnetosphere occupying a larger volume than it would in reality. Also, since the currents are holding the magnetic field structure together, the weaker inner magnetosphere currents in the simulation allow for a faster response of the magnetic field configuration to the SCW. This means that the dipolarization from the SCW will spread faster in the simulation because there is

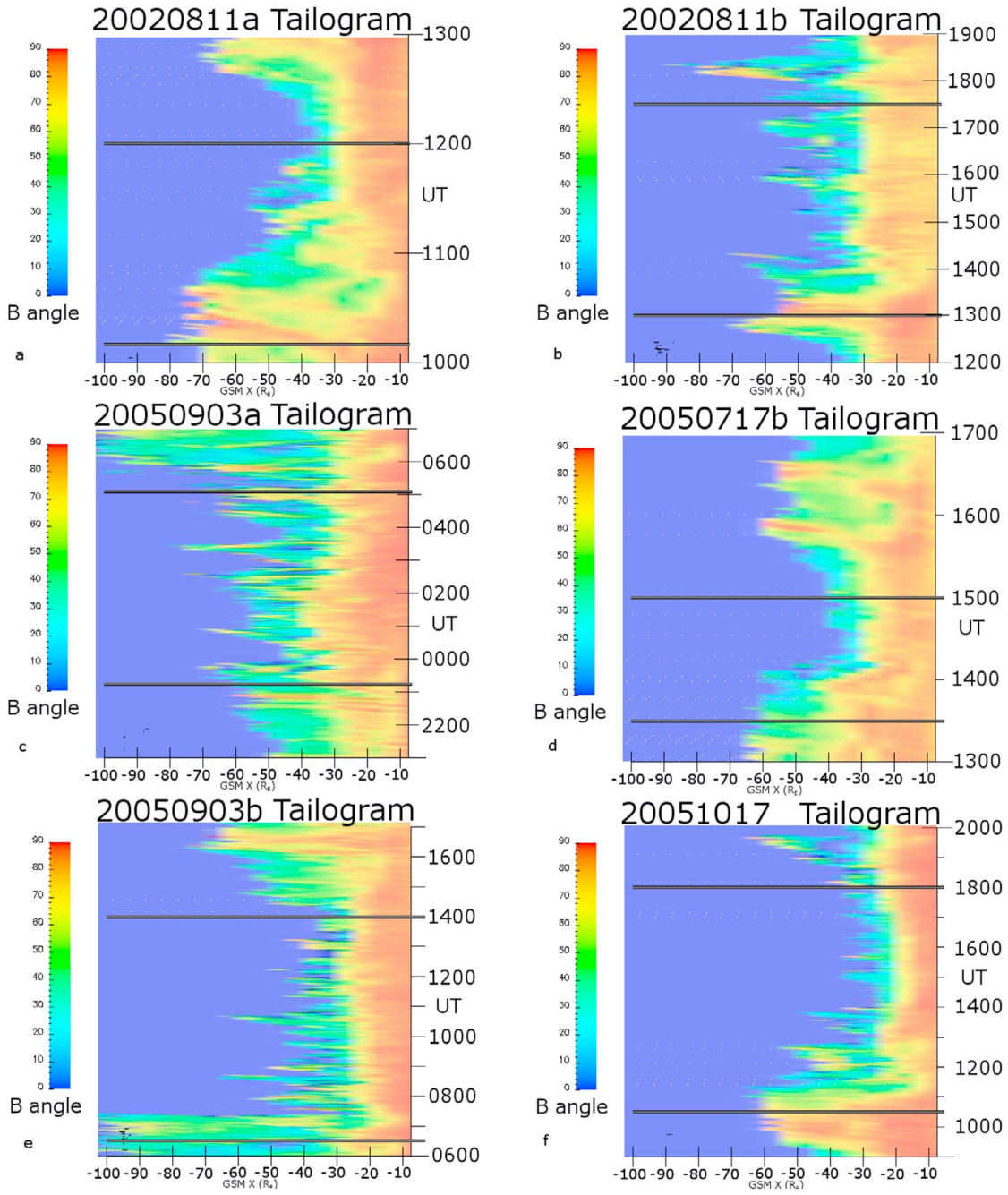

Figure 16. These are the tailograms for the other substorms. It uses the same format as Figure 2.

less current resisting the reconfiguration. For almost all of the measurements of the magnetic field angle presented in section 3.3.2 it is the case that the virtual satellite observed the dipolarization prior to the data. Only in the case of GOES 12 during substorm 20050903a does the simulation and the data see the dipolarization at the same time. This difference in location of the NENL could have an effect on the motion of the neutral line, if there is different behavior for a neutral line formed at $-20\ R_E$ compared to one formed at $-30\ R_E$.

5.2. Simulation Discussion

[56] The substorm growth phase is a period defined by the storage of energy from the solar wind in the magnetotail and a reconfiguration of the magnetosphere. Section 1.1 discussed the signatures of the substorm growth phase that are observed. Among those are an increase in the amount of open magnetic flux in the tail that results in a increasing polar cap and increasing in size of the magnetosphere, a stretching of the magnetic field in the tail, a increase in the total pressure in the tail, and a thinning of the plasma sheet.

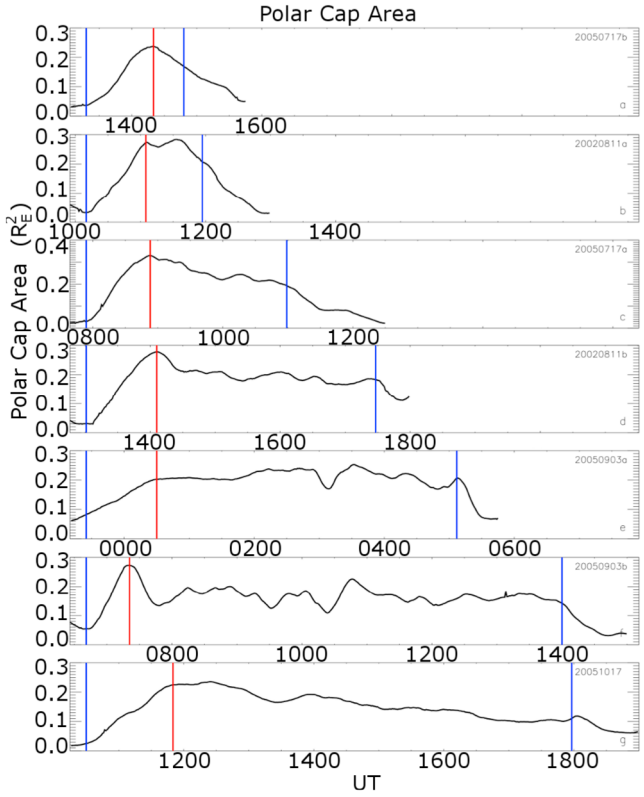

Figure 17. The polar cap area as calculated from the Northern Hemisphere is shown for all seven substorms The polar cap is the area at Earth where the magnetic field is connected to the IMF and is displayed in R_E^2. The vertical blue lines show the beginning and end of each period of southward IMF. The vertical red lines indicate the end times of the initial polar cap growth period.

By observing these parameters for this behavior and identifying when these growth phase observations change, the transition of the magnetosphere from the substorm growth phase to the substorm expansion phase can be identified. This transition also is marked by the presence of the NENL onset. These six signatures are readily seen in the data presented in section 4.2. Table 3 summarizes the transitions observed in those parameters in terms of time after the southward IMF turning.

[57] The "Onset Average" line shows the average of the times for each substorm. These features all show fairly consistent agreement with each other and among the different substorms. The average of all of these signatures across the substorms is 56 ± 14 minutes. This is right in the range of the 45–60 minutes typically given for a substorm growth phase [*Baker et al.*, 1996]. In this paper, all six of the expected features described here were seen in each event simulation, with the one exception that an increase in total pressure in the magnetotail during the growth phase was not seen during substorm 20050903b. Since the growth phase is a loading of energy from the solar wind into the magnetosphere, it is useful to look at the solar wind parameters just for the growth phase for each substorm. Table 4 shows the average value of the solar wind parameters during the growth phase for each substorm, along with the correlation between that parameter and the length of the growth phases. The correlations with the duration of the growth phase of 0.77 for the solar wind velocity and −0.64 for the epsilon parameter suggest that they may be related to the differences in duration of the growth phases. With the epsilon parameter representing the rate of energy transfer from the solar wind to the magnetosphere and growth phase being a storage period for this energy, a connection here implies that there is a minimum amount of energy needed to start a substorm. The last row in Table 4 displays the epsilon parameter integrated over the length of the growth phase, giving an estimate for the total amount of energy input to the magnetosphere. The range of energy is 0.7–2.2 10^{15} J, so while 0.7 10^{15} J may represent the minimum energy needed to initiate a substorm, the average energy input (1.5 ± 0.5 10^{15} J) shows a greater variation than average duration (56 ± 14 minutes), indicating that the onset of the expansion phase is not solely determined by the amount of energy input during the growth phase.

[58] The reproduction of the different growth phase signatures by the simulation as well as the consistency of duration of the growth phase that matches the length expected from observations, supports the view that the simulation is accurately reproducing the loading of energy from the solar wind into the magnetotail and reconfiguration of the magnetosphere experienced during the growth phase.

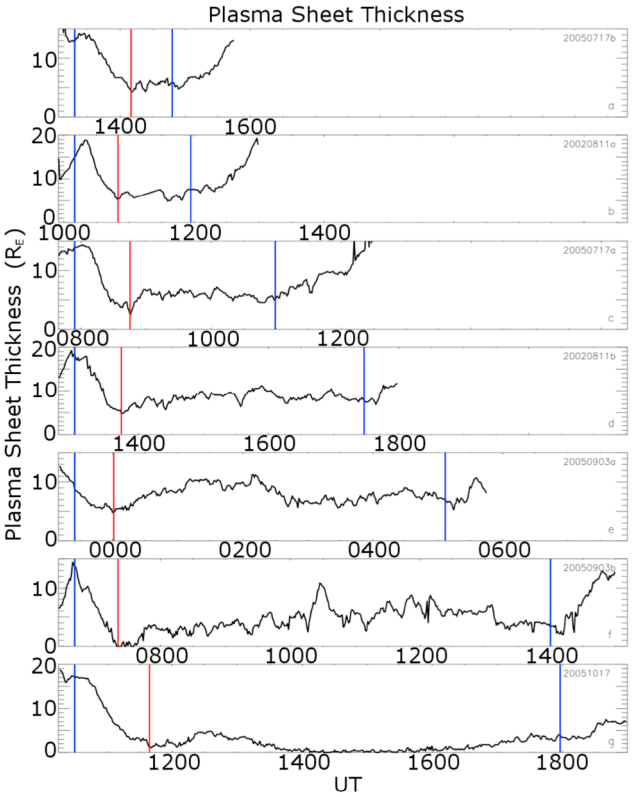

Figure 18. The thickness of the plasma sheet in the z dimension as measured at −20 R_E is shown for all seven substorms. The vertical blue lines show the beginning and end of each period of southward IMF. The vertical red lines indicate the time of the minimum thickness.

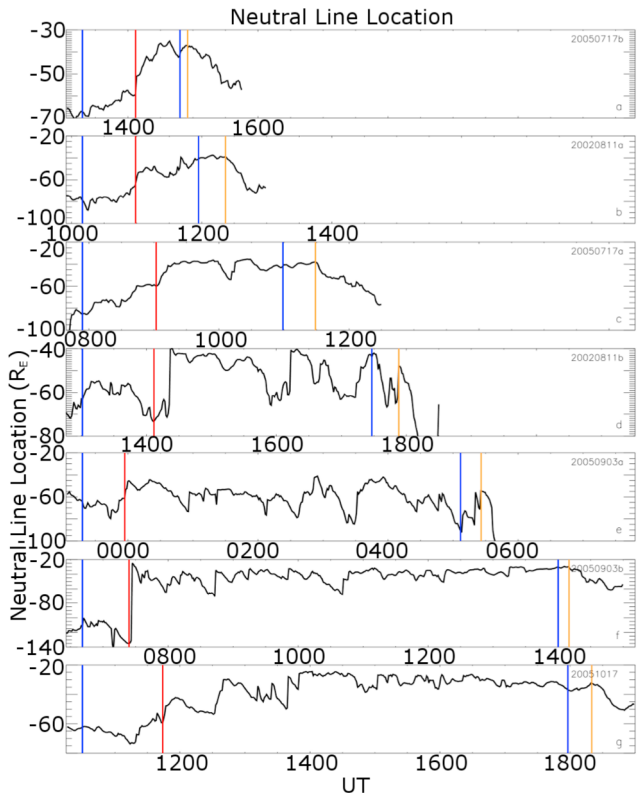

Figure 19. The location of the neutral line is shown for all seven substorms. The vertical blue lines show the beginning and end of each period of southward IMF. The vertical red lines indicate the time near onset when the neutral line jumps earthward and the time when it begins its retreat to the distant neutral line location during quiet time.

[59] Looking at the time of the maximum in the hemispheric power (row 9 in Table 3), which represents the start of the recovery phase in the ionosphere as described in section 1.3, there is a much larger variation (181 ± 63 minutes) than the start of the expansion phase, when compared with the start of the IMF southward period. Substorms 20050717b and 20020811a which had the shortest periods of southward IMF are the only two where the hemispheric power reached a maximum after the IMF turned northward, with the other five substorms reaching a maximum prior to the IMF turning northward. These two also have the shortest period of time from IMF southward to maximum hemispheric power, suggesting that the turning off of the solar wind driver may have caused them to occur earlier than they otherwise would have. Also, the retreat of the neutral line (row 11 in Table 3) shows strong variation (289 ± 148 minutes) when compared to the start of the IMF southward, but it consistently occurs shortly (20 ± 8 minutes) after the IMF turns northward.

[60] Looking at the tailograms (Figures 2 and 16) during the periods of tail activity, there is a relatively consistent location of the boundary between the dipolar region of the inner magnetosphere and the more stretched fields closer to the neutral line at about −30 R_E. During the growth phases of substorms 20020811a, 20050717a and 20051017 there is substantial stretching of a large portion of the inner magnetosphere. Substorms 20020811b and 20050903b also show stretching of the inner magnetosphere, although the stretching does not extend as far earthward as in the previous group. Substorms 20050717b and 20050903a show minimal stretching of inner magnetosphere. The tailograms also show that for substorms 20020811b, 20050903a, and 20059093b there is substantial variation in the location of the neutral line prior to the final tail retreat. Analysis of walkthroughs for those substorms like the one described for substorm 20050717a show that this motion of the neutral line is primarily due to the formation and release of smaller plasmoids after the initial large release caused the expansion onset of the substorm.

[61] For the retreat of the neutral line in each of the substorms, it is clear that it is not connected to the tailward motion of the dipolar region of the magnetosphere. In each event the newly elongated tail is stretched and then subsequently becomes more dipolar in substorms 20050717b, 20020811a, 20050717b, 20020811b and 20050903b, while substorms 20050903a and 20051017 do not show the tail becoming dipolar after stretching, possibly due to subsequent activity after the tail retreat.

[62] The substorm walkthrough in section 3.2 presents a single event view of the LFM simulation of a substorm. It demonstrates the ability of the model to reproduce expected substorm observations as well as emphasizes the potentially cross-tail asymmetry that can occur during a substorm. During the walkthrough of substorm 20050717a, the asymmetry manifests itself in the onset of the NENL, which initially is exclusively on the dawn half of the magnetotail, with the initial flows associated with onset being very different depending on the location in y of the observation. This result show that substorms can be more complicated that the basic 2-D picture given by substorm phenomenological models. This aspect of substorm asymmetry in the tail was also shown in a simulation of a plasmoid flux rope by *Farr et al.* [2008].

6. Conclusions

[63] In summary, this paper has used the simulations of seven different substorms to look at the question of what causes the tailward retreat of the neutral line which defines the start of the recovery phase in the magnetotail. The substorms have a range of different solar wind inputs and when using the AL index to compare the simulation with data from the real event, it is found that the timings, using the correlation with the AL index as validation, are reproduced fairly well. By comparing the various signatures of the substorm growth phase and expansion onset, the simulation recreated those signatures with a duration of the growth phase that matches with the expected behavior from substorm observations.

[64] Using the comparison of the simulation with satellite data, it can be seen that a weakness of the simulation is that the inner magnetosphere does not experience much stretching of the magnetic field, but is instead relatively dipolar. From the satellite comparisons this difference in magnetic field was about 20°. Another weakness is that the entire inner magnetosphere dipolarizes quickly at substorm onset in the simulation. Also the NENL usually forms at −30 to −40 R_E in the

Table 3. Times for the Substorm Simulations[a]

Event	20050717b	20020811a	2005050717a	20020811b	20050903a	20050903b	20051017	Average
IMF south begin	1318 UT	1010 UT	0754 UT	1301 UT	2318 UT	0641 UT	1030 UT	
PS thinning end	52	40	51	43	43	39	69	48 ± 10
MS thickening end	71	74	61	64	64	47	89	67 ± 13
Tail dipolarization	40	55	43	54	41	39	71	49 ± 12
Max Tail Pressure	45	60	63	67	52	-	63	58 ± 8
PCA growth end	61	56	59	65	72	40	80	61 ± 11
NENL onset	49	49	68	66	39	43	74	54 ± 14
Onset average	53 ± 11	56 ± 11	58 ± 9	60 ± 9	52 ± 14	42 ± 3	74 ± 9	56 ± 13
Max Hemispheric Power	112	120	182	190	288	141	244	182 ± 63
IMF south end	90	107	185	267	339	439	448	269 ± 148
NENL retreat	97	132	246	292	368	454	470	290 ± 148
IMF north to NENL retreat	7	25	30	25	19	10	22	20 ± 8

[a]All durations in minutes.

simulation instead of the typically observed location closer to −20 R_E. These differences are probably related in that a NENL needs stretched field conditions to occur; therefore, if the magnetic field was stretched more in the inner magnetosphere, magnetic reconnection could take place closer in to Earth. It is possible that the onset dipolarization would not encompass as large of a region with the NENL closer to the Earth because of the strong currents keeping the magnetic field more stretched, slowing the spread of the dipolarization.

[65] With regard to the tailward retreat of the neutral line, the simulation does not show a connection with the dipolarization of the inner magnetosphere. Instead, the neutral line retreats after the solar wind driver has been turned off. This is in contrast to the results presented in section 1.3 by *Baumjohann et al.* [1999]. Two possible reasons for the different are postulated here.

[66] First, *Baumjohann et al.* [1999] does not discuss the solar wind conditions for the events used in the superposed epoch study. Since several of the substorms of this paper are longer than the average substorm length due to the lengthy periods of southward IMF, it is possible that they are separating the dipolarization of the inner magnetosphere from the tailward retreat of the neutral line that might otherwise be much closer together. For instance, the substorm in this paper with the shortest period of southward IMF, substorm 20050717b, had the retreat of the neutral line occurring 45 minutes after substorm onset, which is exactly in agreement with the result in Baumjohann.

[67] The second possible explanation is that the data used by *Baumjohann et al.* [1999] is from the Geotail spacecraft over a range of tail location from −11 to −31 R_E. As stated previously, the simulation typically generates a NENL at greater than −30 R_E. If the simulation generated a NENL at a more earthward location, it is possible that a connection between dipolarization and the location of the reconnection site may be seen in the simulation.

[68] There are two follow-ups to the result presented in this paper that will be the focus of future investigations. A study looking at the connection between the location of the neutral line and the solar wind conditions will be performed. A first step in this investigation will be to see if there is solar wind data available for the events used in the epoch study by *Baumjohann et al*. [1999]. It will also be useful to use a multisatellite constellation such as the THEMIS mission [*Sibeck and Angelopoulos*, 2008] to more accurately observe the tailward retreat of the neutral line. If this study showed no correlation between the northward turning of the IMF and the retreat of the neutral line, then the results taken from the simulation here would be wrong and it will be a useful point of comparison to future versions of the model to see if the result changes. If this study does show a correlation, then a means of reconciling this result with the *Baumjohann et al.* [1999] results would be needed. One possibility would be that under continued solar wind driving, the piled-up magnetic flux would continue around to the dayside of the magnetosphere and could then be cycled through the reconnection cycle again. This would allow for the flux to not keep piling up solely on the nightside of the magnetosphere.

[69] Another avenue for investigation is that the LFM model is undergoing a variety of advancements to improve the quality of its reproduction of the near-Earth space environment. Among these are the transition to a multifluid version which allows for the presence of other species of ions and/or populations of ions with different temperatures, the addition of ionospheric outflow from Earth, and the joining with the Rice Convection Model (RCM), an inner magnetosphere model of the ring current and plasmasphere. The initial work on these changes have been shown to have

Table 4. Average Values for the Solar Wind During the Growth Phase for Each Substorm

	20050717b	20020811a	2005050717a	20020811b	20050903a	20050903b	20051017	Correlation
Growth phase (min)	53 ± 12	56 ± 11	58 ± 9	60 ± 9	52 ± 14	42 ± 3	74 ± 9	56 ± 13
Density (cc)	14.5	9.1	9.8	6.8	9.0	2.2	5.5	0.05
V_x (km/s)	−445	−456	−493	−462	−667	−625	−376	0.77
B_z	−4.3	−3.8	−6.6	−6.2	−2.0	−3.8	−2.6	0.02
Epsilon (10^{11} W)	4.5	3.6	6.2	4.7	6.6	4.8	1.5	−0.64
Integrated Epsilon (10^{15} J)	1.4	1.2	2.2	1.7	1.8	1.2	0.7	

an effect on the location of the NENL in a substorm simulation, as shown by *Wiltberger et al.* [2010], and the joining with the RCM in particular will enhance the currents in the inner magnetosphere, thereby creating more stretching of the magnetic field in the near-tail region. Performing a similar study using newer versions of the LFM may result in changes to the result observed here, especially if the more advanced model results in a NENL forming closer to Earth.

[70] In conclusion, this work represents one of the larger studies for MHD simulation of substorms, in terms of the number of different events simulated. It accurately reproduces the timing and features of the substorm growth phase and expansion phase onset as a storage and release of energy in the magnetotail, not as directly driven by the solar wind. Detailed analysis of the plasmoid flux rope generated during one of the events shows how the fully 3-D nature of a global MHD model can enhance the understanding of the complicated behavior of a flux rope during a substorm. Observations of the location and evolution of the neutral line during the substorm reveals the result that the retreat of the neutral line is a process directly driven by the solar wind. When the southward IMF that is driving the substorm is turned off, the neutral line begins the tailward retreat, which is the start of the substorm recovery phase.

[71] **Acknowledgments.** This research was undertaken with the support of the Center for Integrated Space Weather Modeling via NSF STC grant ATM-0120950. This research was also supported by the National Center for Atmospheric Research, which is sponsored by the National Science Foundation.

[72] Masaki Fujimoto thanks Tiera Laitinen and an anonymous reviewer for their assistance in evaluating this paper.

References

Akasofu, S.-I. (1964), The development of the auroral substorm, *Planet. Space. Sci.*, *12*, 273–282.

Baker, D. N., T. I. Pulkinnen, E. W. Hones Jr., R. D. Belian, R. L. McPherron, and V. Angelopoulos (1994), Signatures of the substorm recovery phase at high-altitude spacecraft, *J. Geophys. Res.*, *99*, 10,967–10,980.

Baker, D. N., T. I. Pulkinnen, V. Angelopoulos, W. Baumjohann, and R. L. McPherron (1996), Neutral line model of substorms: Past results and present view, *J. Geophys. Res.*, *101*, 12,975–13,010.

Baker, D. N., T. I. Pulkinnen, J. Buchner, and A. J. Klimas (1999), Substorms: A global instability of the magnetosphere-ionosphere system, *J. Geophys. Res.*, *104*, 14,601–14,611.

Baumjohann, W., M. Hesse, S. Kokubun, T. Mukai, T. Nagai, and A. A. Petrukovich (1999), Substorm dipolarization and recovery, *J. Geophys. Res.*, *104*, 24,995–25,000.

Brittnacher, M., M. Fillingim, and G. Parks (1999), Polar cap area and boundary motion during substorms, *J. Geophys. Res.*, *104*, 12,251–12,262.

Bryant, C. R. (2008), In-depth analysis of the substorm recovery phase using electron and proton induced emissions from satellite observations, Ph.D. thesis, Univ. of Calgary, Calgary, Alberta, Canada.

Farr, N. L., D. N. Baker, and M. Wiltberger (2008), Complexities of a 3-D plasmoid flux rope as shown by an MHD simulation, *J. Geophys. Res.*, *113*, A12202, doi:10.1029/2008JA013328.

Koskinen, H. E., and E. I. Tanskanen (2002), Magnetospheric energy budget and the epsilon parameter, *J. Geophys. Res.*, *107*(A11), 1415, doi:10.1029/2002JA009283.

Laitinen, T. V., T. I. Pulkinnen, M. Palmroth, P. Janhunen, and H. E. J. Koskinen (2005), The magnetotail reconnection region in a global MHD simulation, *Ann. Geo.*, *23*, 3753–3764.

Lopez, R. E., C. C. Goodrich, M. Wiltberger, and J. G. Lyon (1998), Simulation of the March 9, 1995 substorm and initial comparison to data, in *Geospace Mass and Energy Flow: Results From the International Solar-Terrestrial Physics Program*, *Geophys. Monogr. Ser.*, vol. 104, edited by D. L. Gallagher, J. L. Horwitz, and W. K. Peterson, 237 pp., AGU, Washington, D. C.

Lui, A. T. Y. (1996), Current disruption in the Earth's magnetosphere: Observations and models, *J. Geophys. Res.*, *101*, 13,067–13,088.

Lyon, J. G., J. A. Fedder, and C. M. Mobarry (2004), The Lyon-Fedder-Mobarry (LFM) global MHD magnetospheric simulation code, *J. Atm. Space Phys.*, *66*, 1333–1350.

McPherron, R. L., C. T. Russell, and M. Aubry (1973), Satellite studies of magnetospheric substorms on August 15, 1968: Phenomenological model for substorms, *J. Geophys. Res.*, *78*, 3131–3149.

Opgenoorth, H. J., M. A. L. Persson, T. I. Pulkkinen, and R. J. Pellinen (1994), Recovery phase of magnetospheric substorms and its association with morning-sector aurora, *J. Geophys. Res.*, *99*, 4115–4129.

Petrukovich, A. A., W. Baumjohann, R. Nakamura, and A. Runov (2007), Thinning and stretching of the plasma sheet, *J. Geophys. Res.*, *112*, A10213, doi:10.1029/2007JA012349.

Pulkkinen, T. I., R. J. Pellinen, H. E. J. Koskinen, H. J. Opgenoorth, J. S. Murphree, V. Petrov, A. Zaitzev, and E. Friis-Christensen (1991), Auroral signatures of substorm recovery: A case study, in *Magnetospheric Substorms*, *Geophys. Monogr. Ser.*, vol. 64, edited by J. R. Kan, T. A. Potemra, S. Kokubun, and T. Iijima, pp. 333–341, AGU, Washington, D. C.

Pulkkinen, T. I., D. N. Baker, P. K. Toivanen, R. J. Pellinen, R. H. W. Friedel, and A. Korth (1994), Magnetospheric field and current distributions during the substorm recovery phase, *J. Geophys. Res.*, *99*, 10,955–10,966.

Raeder, J., and R. L. McPherron (1998), Global MHD simulations of the substorm current wedge and dipolarization, in *Substorms-4: International Conference on Substorms-4, Lake Hamana, Japan, March 9–13, 1998*, edited by S. Kokubun and Y. Kamide, p. 343, Terra Sci., Tokyo.

Sibeck, D. G., and V. Angelopoulos (2008), THEMIS science objectives and mission phases, *Space Sci. Rev.*, *141*, 35–59.

Tanskanen, E. I., A. T. Viljanen, T. I. Pulkkinen, R. J. Pirjola, L. V. T. Häkkinen, A. A. Pulkkinen, and O. Amm (2001), At substorm onset, 40% of AL comes from underground, *J. Geophys. Res.*, *106*, 13,119–13,134.

Toth, G., et al. (2005), Space weather modeling framework: A new tool for the space science community, *J. Geophys. Res.*, *110*, A12226, doi:10.1029/2005JA011126.

Walker, R. J., and T. Ogino (1996), A global magnetohydrodynamic simulation of the origin and evolution of magnetic flux ropes, *J. Geomag. Geoelec.*, *48*, 765–779.

Weimer, D. R., D. M. Ober, N. C. Maynard, M. R. Collier, D. J. McComas, N. F. Ness, C. W. Smith, and J. Watermann (2003), Predicting interplanetary magnetic field (IMF) propagation delay times using the minimum variance technique, *J. Geophys. Res.*, *108*(A1), 1026, doi:10.1029/2002JA009405.

Wiltberger, M., T. I. Pulkinnen, J. G. Lyon, and C. C. Goodrich (2000), MHD simulation of the December 10, 1996 substorm, *J. Geophys. Res.*, *106*, 27,649–27,663.

Wiltberger, M., R. S. Weigel, W. Lotko, and J. A. Fedder (2009), Modeling seasonal variations in auroral particle precipitation, *J. Geophys. Res.*, *114*, A01204, doi:10.1029/2008JA013108.

Wiltberger, M., W. Lotko, J. Lyon, P. A. Damiano, and V. G. Merkin (2010), Influence of cusp O+ outflow on magnetotail dynamics in a multifluid MHD model of the magnetosphere, *J. Geophys. Res.*, *115*, A00J05, doi:10.1029/2010JA015579.

D. N. Baker and N. L. Farr, Laboratory for Atmospheric and Space Physics, University of Colorado at Boulder, 1234 Innovation Dr., Boulder, CO 80303, USA. (daniel.baker@lasp.colorado.edu; nathan.farr@colorado.edu)

M. Wiltberger, National Center for Atmospheric Research, High Altitude Observatory, 3080 Center Green, Boulder, CO 80301, USA. (wiltbemj@ucar.edu)